

RESEARCH ARTICLE

Simulation of orthogonal horizontal components of near-fault ground motion for specified earthquake source and site characteristics

Mayssa Dabaghi¹  | Armen Der Kiureghian^{2,3}

¹ American University of Beirut, Beirut, Lebanon

² American University of Armenia, Yerevan, Armenia

³ University of California, Berkeley, CA, USA

Correspondence

Mayssa Dabaghi, Assistant Professor, American University of Beirut, Beirut, Lebanon.

Email: mayssa.dabaghi@aub.edu.lb

Funding information

California Department of Transportation (Caltrans), Grant/Award Number: 59A0582; Pacific Earthquake Engineering Research Center (PEER) Transportation Systems Research Program; Pacific Gas & Electric Company; Taisei Chair in Civil Engineering at the University of California, Berkeley

Summary

A procedure to generate horizontal pairs of synthetic near-fault ground motion components for specified earthquake source and site characteristics is presented. Some near-fault ground motions contain a forward directivity pulse; others do not, even when the conditions for such a pulse are favorable. The proposed procedure generates pulse-like and non-pulse-like motions in appropriate proportions. We use our recent stochastic models of pulse-like and non-pulse-like near-fault ground motions that are formulated in terms of physically meaningful parameters. The parameters of these models are fitted to databases of recorded pulse-like and non-pulse-like motions. Using these empirical “observations,” predictive relations are developed for the model parameters in terms of the earthquake source and site characteristics (type of faulting, earthquake magnitude, depth to top of rupture plane, source-to-site distance, site characteristics, and directivity parameters). The correlation coefficients between the model parameters are also estimated. For a given earthquake scenario, the probability of occurrence of a directivity pulse is first computed; pulse-like and non-pulse-like motions are then simulated according to the predicted proportions using the empirical predictive models. The resulting time series are realistic and reproduce important features of recorded near-fault ground motions, including the natural variability. Moreover, the statistics of their elastic response spectra agree with those of the NGA-West2 dataset, with the additional feature of distinguishing between pulse-like and non-pulse-like cases and between forward and backward directivity scenarios. The synthetic motions can be used in addition to or in place of recorded motions in performance-based earthquake engineering, particularly when recorded motions are scarce.

KEYWORDS

multi-component synthetic motions, near-fault ground motions, NGA database, pulse-like motions, rupture directivity, stochastic models

1 | INTRODUCTION

Synthetic ground motions have long been of interest in the field of earthquake engineering. Moreover, recently, there has been increased effort in characterizing near-fault ground motions. These motions tend to be more complex and more variable than far-field ground motions and may possess distinct characteristics including the rupture directivity effect in the fault-normal (FN) direction and the “fling step” in the fault-parallel (FP) direction.^{1–3} See our recent paper⁴ for a brief review of the characteristics of near-fault ground motions. These characteristics can have strong influence on the performance of structures located at near-fault sites.^{5–10} As a result, methods for generation of synthetic *near-fault* ground motions are of growing interest.

Synthetic near-fault ground motions can be used for a variety of engineering applications, including for nonlinear dynamic analysis of structures located at near-fault sites. Such structures can be particularly vulnerable to near-fault motions if they possess resonant periods that are long and close to the period of the directivity pulse. Furthermore, a suite of synthetic motions can be used in performance-based earthquake engineering (PBEE), where estimates of expected costs of damage or downtime must be made. Probabilistic seismic hazard analysis (PSHA), the first and fundamental step of PBEE, requires a ground motion model. Many types of ground motion models are available; see our recent paper⁴ for a brief review. In the conventional approach to PSHA, ground motion prediction equations (GMPEs) are used, and the hazard at a site is represented by a response spectrum. This approach is not adequate if the structure is expected to respond in its nonlinear range. Alternatively, models of ground motion time series can be used, and the seismic hazard directly characterized in terms of synthetic ground motions instead of a response spectrum.^{11,12} This approach offers a more accurate description of the structural response because it provides joint knowledge of more than one ground motion parameter.¹³

Our objective is to generate synthetic near-fault ground motions for a specified earthquake scenario. Obviously, it is crucial that the synthetic motions be realistic and capture the important characteristics of real recorded near-fault ground motions, including temporal and spectral nonstationarity, near-fault effects, and the characteristics that control the response of structural and geotechnical systems, namely, the intensity, duration, and frequency content characteristics and their evolution in time. Because of the moving resonance effect in inelastic structures,¹⁴ these features are essential when models of ground motion time series are used in nonlinear dynamic analysis. Moreover, near-fault ground motion models should consider both *pulse-like* and *non-pulse-like* motions because not all near-fault ground motions contain a forward directivity (FD) pulse, even when the conditions for such a pulse are favorable.^{15,16} Finally, for PSHA, it is crucial that synthetic motions properly represent the natural variability of real recorded motions for given earthquake source and site characteristics.

Many models have been proposed in the literature to generate synthetic near-fault ground motion time series. They include source-based deterministic models,^{1,17,18} source-based stochastic models,^{19–21} site-based stochastic models,^{4,22–25} and hybrid models.²⁶ Although these models are able to represent both pulse-like and non-pulse-like motions, many have focused on representing and fitting only the more damaging *pulse-like* motions. For engineering applications, stochastic and hybrid ground motion models are generally of more interest because they are able to represent a wider range of the frequencies that are present in recorded ground motions. Stochastic models of *pulse-like* near-fault ground motion may also be classified as hybrid. They consist of the summation of a low-frequency component, the pulse motion, and a broadband or high-frequency component, the residual motion. The pulse motion is modeled using a deterministic waveform^{4,19–23} or a narrowband stochastic process.^{24,25} The residual motion is modeled using a source-based^{19–21} or a site-based^{4,22–25} stochastic model.

Most stochastic models of near-fault ground motion have been fitted to specific events or target records and are able to generate synthetic ground motions with characteristics similar to those of the target event or record. However, some of these models^{22,23} do not account for spectral nonstationarity. On the other hand, the models in Mavroeidis and Papageorgiou¹⁹ and Halldórsson et al.,²⁰ which are based on the specific barrier model,²⁷ can represent spectral nonstationarity because the source is modeled as an aggregate of subevents, where each subevent results in a time series having arrival time and frequency content that depend on the subevent rupture time and subevent-site geometry. The subevent time series are then combined to obtain the total ground motion at a site, resulting in a nonstationary process. To generate synthetic ground motions from hypothetical events for PBEE applications, predictive relations that account for the variability of all the model parameters and for the correlations between them are necessary. Such relations can be developed for parametrized models by fitting them to a catalog of recorded motions and performing statistical analysis. However, some previous attempts in this direction have failed to fully account for the variability of all the model parameters^{21–23} or for the correlations between them.^{19–23} Furthermore, some site-based models characterize only the

directivity pulse and were fitted to recorded near-fault ground motions.^{15,28–30} Predictive relations are developed for the parameters of some of these pulse models.^{15,31,32} However, these models lack the high frequency content of real ground motions. Predictive relations that account for the natural variability of the parameters of the pulse model in Mavroeidis and Papageorgiou¹⁹ have been recently presented in Halldórsson et al and Cork et al.^{20,33}

In our previous work,⁴ we developed a site-based parameterized stochastic model of near-fault ground motion in 2 orthogonal horizontal directions. The model is defined in terms of a set of physically meaningful parameters that represent the major characteristics of recorded near-fault ground motions. It accounts for the near-fault effects of rupture directivity and the fling step, although the main focus is on the former, and it considers both pulse-like and non-pulse-like motions. A method to fit the model parameters to recorded near-fault ground motions was presented in Dabaghi and Der Kiureghian.⁴ Moreover, a procedure to generate and postprocess synthetic motions for specified model parameters was described in that reference and used to generate synthetic ground motions that possess characteristics similar to recorded near-fault ground motions. See⁴ for a list of the advantages of the proposed model.

In this paper, we present a procedure to use our previous model⁴ to generate suites of horizontal pairs of synthetic near-fault ground motions for specified earthquake scenarios. The paper begins with a brief review of the characteristics of near-fault ground motions, followed by a summary of the stochastic models of pulse-like and non-pulse-like near-fault ground motions in Dabaghi and Der Kiureghian.⁴ The model is then fitted to subsets of PEER's NGA-West2 database to obtain empirical "observations" of the model parameters. After transformation to the normal space, empirical predictive equations are constructed for the transformed model parameters in terms of earthquake source and site characteristics that are typically available to the design engineer. These include the type of faulting F , the moment magnitude M_w , the depth Z_{TOR} to the top of the rupture plane, the closest distance R_{RUP} from the site to the fault rupture, the shear-wave velocity V_{s30} of the site, and directivity parameters $s_{or}d$ and $\theta_{or}\phi$ that describe the geometric configuration of the site relative to the rupture surface. Moreover, the variability of the parameters and the statistical correlation between them are estimated. These correlations describe the relations between pairs of model parameters after having removed the effect of common predictor variables. Next, the procedure for generating a suite of ground motions for specified earthquake source and site characteristics is described. For a specified earthquake scenario, first, the predictive relations are used to simulate sample realizations of the model parameters. The simulated model parameters are then used in conjunction with the procedure presented in Dabaghi and Der Kiureghian⁴ to generate synthetic near-fault ground motions for the earthquake scenario of interest. An empirical model of the probability of occurrence of the directivity pulse³⁴ is used to generate pulse-like and non-pulse-like ground motions in appropriate proportions. The resulting motions have realistic time series and are able to reproduce the important features of recorded near-fault ground motions, including the natural variability. Finally, the proposed simulation procedure is validated by generating families of synthetic near-fault ground motions and comparing the statistics of their elastic response spectra with those of the NGA-West2 GMPEs.^{35,36} A more detailed account of the procedures and results presented in this paper can be found in Dabaghi and Der Kiureghian.³⁷

The proposed simulation procedure has the following characteristics: (1) It provides synthetic near-fault ground motions in 2 orthogonal horizontal directions; (2) the synthetics properly represent the temporal and spectral characteristics and nonstationarities of the near-fault ground motion; (3) pulse-like and non-pulse-like synthetic ground motions are generated in appropriate proportions; (4) the model parameters are predicted for specified earthquake source and site characteristics while fully accounting for the variability of the parameters and for the correlations between them; (5) the synthetics are able to reproduce the variability present in real ground motions; and (6) the fling step is easily incorporated into the formulation.

2 | CHARACTERISTICS OF NEAR-FAULT GROUND MOTION

Important engineering characteristics of a ground motion at a site are measures of the intensity, duration, and frequency content. In the near-fault region, defined here as the region within 30 km of the fault rupture, ground motions may additionally be characterized by 2 important near-fault effects: the directivity effect and the fling step. The directivity effect depends on the spatial distribution of the slip along the fault rupture, on the radiation pattern between the fault rupture and the site, and on the velocity and direction of propagation of the rupture relative to the site.¹ The FD effect occurs when the rupture front propagates towards the site and at a velocity almost equal to the shear-wave velocity of the ground, so that all the seismic energy radiated from the fault rupture arrives at the site in a single, short-duration pulse.

Sites located in the FD region may experience a two-sided, large-amplitude, short-duration pulse at the beginning of the velocity time series, in the FN direction (the direction perpendicular to the fault plane).^{1,2,38} If the rupture propagates away from the site, the site is said to be in the backward directivity (BD) region and typically records a small amplitude, long-duration ground motion in the FN direction.² The “fling step” occurs at sites that undergo a permanent static ground displacement due to the relative movement of the 2 sides of a rupturing fault. This effect typically appears in the FP direction, as a step function in the displacement time series and as a one-sided pulse in the velocity time series.^{3,39}

Not all near-fault ground motions contain a directivity pulse, even when they are recorded in the FD region. Conversely, near-fault sites may record a directivity pulse even when they are not in a geometric configuration that is favorable for such an event.¹⁵ Moreover, the pulse-like features from the directivity effect are observed in a range of orientations, which often but not always include the strike-normal (SN) orientation. And even if a directivity pulse occurs in the SN direction, the largest pulse might occur in a different direction.¹⁶ This variability is inherent to earthquake ground motions and results from the complex nature of the rupture propagation and variability of the velocity structure of the ground.³ Note that we distinguish between the FN and the SN directions, and between the FP and the strike-parallel (SP) directions. See Dabaghi and Der Kiureghian^{4,37} for more details.

In this and our previous work,^{4,37} the characterization of a ground motion as pulse-like or non-pulse-like refers to the presence or absence of a *directivity* pulse and is independent of the “fling” step. Note that pulses due to the fling step are absent from the ground motion records used in this work because they are removed by standard filtering and baseline correction procedures. A ground motion is classified as pulse-like if at least one of its horizontal components is pulse-like; otherwise, it is classified as non-pulse-like.¹⁶ Note the distinction between the classifications as pulse-like or non-pulse-like of a *ground motion* versus a *ground motion component*. Identification of the directivity pulse is not a straightforward task.⁴⁰ The definition of what constitutes a pulse and what defines the boundary between pulse-like and non-pulse-like motions is somewhat subjective. In our work, ground motion records are classified as either pulse-like or non-pulse-like following the method developed by Shahi and Baker,¹⁶ which is based on a wavelet signal processing method proposed by Baker.⁴¹ More recently, the same authors proposed another version of the classification algorithm,³⁴ but this study uses the old version.

3 | STOCHASTIC MODEL OF NEAR-FAULT GROUND MOTION

Our stochastic model in Dabaghi and Der Kiureghian⁴ describes near-fault ground acceleration in 2 orthogonal horizontal directions and accounts for the pulse-like and non-pulse-like cases. The model combines submodels that are summarized below. It is formulated in terms of physically meaningful parameters that characterize the main features of recorded near-fault ground motions. For more details, see Dabaghi and Der Kiureghian.^{4,37}

3.1 | Model of the directivity pulse

The directivity pulse is modeled in the velocity domain using the modified Mavroëdis-Papageorgiou (mMP) pulse; see Mavroëdis and Papageorgiou¹⁹ and Dabaghi et al.⁴² The mMP pulse is defined by

$$v_{pul}(t) = \begin{cases} \left\{ \frac{1}{2} V_p \cos \left[2\pi \left(\frac{t-t_{max,p}}{T_p} \right) + \nu \right] - \frac{D_r}{\gamma T_p} \right\} \left\{ 1 + \cos \left[\frac{2\pi}{\gamma} \left(\frac{t-t_{max,p}}{T_p} \right) \right] \right\} & t_{i,p} < t \leq t_{f,p}, \\ = 0 & \text{elsewhere,} \end{cases} \quad (1)$$

where the 5 model parameters are the pulse amplitude V_p , the pulse period T_p , parameter γ characterizing the number of oscillations in the pulse, the phase angle ν , and the time of the peak of the envelope $t_{max,p}$. To be precise, V_p is a parameter that controls the amplitude of the velocity pulse; however, its value closely matches the pulse amplitude. In the fitting procedure,⁴ V_p is constrained to the maximum absolute amplitude of the extracted velocity pulse; the remaining parameters are then identified by minimizing the squared difference between the fitted and extracted velocity pulse waveforms. Comparison of the fitted and extracted pulses shows that the fit is satisfactory, see Dabaghi and Der Kiureghian.⁴ The pulse starts at time $t_{i,p} = t_{max,p} - 0.5\gamma T_p$ and ends at time $t_{f,p} = t_{max,p} + 0.5\gamma T_p$. D_r is the nonzero displacement at the end of the pulse in the original formulation,¹⁹

$$D_r = V_p T_p \frac{\sin(\nu + \gamma\pi) - \sin(\nu - \gamma\pi)}{4\pi(1 - \gamma^2)}, \quad (2)$$

and is included in the modified model to achieve zero displacement at the end of the pulse. To overcome the arbitrariness in the start time t_0 of a ground motion, we define $D_{0-max,p} = t_{max,p} - t_0$ as the nominal time to the peak of the pulse. A definition for the nominal start time t_0 , which is assumed to be the same for all components of the ground motion, is presented in Section 3.3. The acceleration of the directivity pulse, $a_{pul}(t)$, is the derivative of $v_{pul}(t)$.

3.2 | Model of broadband near-fault ground motion

Residuals of pulse-like near-fault ground motions after removal of the pulse, as well as near-fault ground motion components that do not contain a pulse, are generally broadband time series with slowly evolving temporal and spectral characteristics. The nonstationary modulated, filtered white-noise (MFW) model formulated by Rezaeian and Der Kiureghian^{43,44} is used to model these broadband motions. The model for the acceleration process is described by

$$a_{MFW}(t) = q(t) \left\{ \frac{1}{\sigma_h(t)} \int_{-\infty}^t h[t-\tau, \lambda(\tau)] w(\tau) d\tau \right\}, \quad (3)$$

where $w(t)$ is a white-noise process, $h[t-\tau, \lambda(\tau)]$ is the unit-impulse response function (IRF) of a linear filter with time-varying parameters $\lambda(\tau) = [\omega_f(\tau), \zeta_f(\tau)]$, $\sigma_h(t)$ is the standard deviation of the process defined by the integral, and $q(t)$ is a time-modulating function that characterizes the root-mean-square of the acceleration process. For the IRF, the form selected in Rezaeian and Der Kiureghian⁴³ is adopted. For near-fault ground motions, the modulating function

$$q(t) = \begin{cases} 0 & t \leq t_{0,q} \\ c \left(\frac{t-t_{0,q}}{t_{max,q}-t_{0,q}} \right)^\alpha & t_{0,q} < t \leq t_{max,q} \\ c \exp[-\beta(t-t_{max,q})] & t_{max,q} < t \end{cases} \quad (4)$$

is selected, where $t_{0,q} = t_0$ and $t_{max,q}$ are the start and peak times, respectively. As described in Dabaghi and Der Kiureghian,⁴ the modulating function parameters ($\alpha, \beta, c, t_{max,q}$) are related to physical quantities of a ground motion component, namely, its Arias intensity, I_a , its effective duration, D_{5-95} (time between 5% and 95% Arias intensity values), and the durations D_{0-5} and D_{0-30} from t_0 to the 5% and 30% Arias intensity values, respectively. For the filter frequency, the linear form used in Rezaeian and Der Kiureghian⁴⁴ is adopted,

$$\omega_f(\tau) = 2\pi[f_{mid} + f'(\tau-t_{mid})], \quad (5)$$

where f_{mid} is the filter frequency in Hz at the middle of the ground shaking t_{mid} , taken as the time t_{30,I_a} of the 30% Arias intensity value of the motion, and f' is the rate of change in Hz/s of the frequency with time. Finally, the filter damping is taken to be a constant, $\zeta_f(\tau) = \zeta_f$. Thus, the 7 physically relevant parameters ($I_a, D_{5-95}, D_{0-5}, D_{0-30}, f_{mid}, f', \zeta_f$) completely define the process representing the broadband near-fault ground acceleration.

3.3 | Stochastic models of pulse-like and non-pulse-like near-fault ground motion

The model of the pulse-like ground acceleration is formulated in the direction of the largest horizontal pulse, $a_{PP}(t)$, and in the corresponding orthogonal direction, $a_{PO}(t)$. The orthogonal component is assumed to be non-pulse-like, ie, not to contain a directivity pulse. The model for $a_{PP}(t)$ is broken down into 2 submodels: one for the directivity pulse, $a_{pul}(t)$, and one for the residual motion, $a_{res}(t)$, which is the total motion minus the pulse. The directivity pulse $a_{pul}(t)$ is modeled using the mMP pulse with parameters ($V_p, T_p, \gamma, \nu, D_{0-max,p}$), while $a_{res}(t)$ and $a_{PO}(t)$ are modeled using the MFW process with parameters ($I_{a,res}, D_{5-95,res}, D_{0-5,res}, D_{0-30,res}, f_{mid,res}, f'_{res}, \zeta_{f,res}$) and ($I_{a,PO}, D_{5-95,PO}, D_{0-5,PO}, D_{0-30,PO}, f_{mid,PO}, f'_{PO}, \zeta_{f,PO}$), respectively. The pulse-like model is thus formulated in terms of 19 parameters denoted $\alpha_{P,i}$, $i = 1, \dots, 19$; see Table 1. Note that to overcome the arbitrariness in the start time t_0 of a ground motion, $\alpha_{P,5} = D_{0-max,p} = t_{max,p} - t_0$ is used here, and not $\alpha_{P,5} = t_{max,p}$ as was done in our earlier work.³⁷

The model of non-pulse-like near-fault ground motion is formulated for the major and intermediate components of acceleration, denoted $a_{NP1}(t)$ and $a_{NP2}(t)$, respectively. These components are modeled using the MFW process with parameters ($I_{a,NP1}, D_{5-95,NP1}, D_{0-5,NP1}, D_{0-30,NP1}, f_{mid,NP1}, f'_{NP1}, \zeta_{f,NP1}$) and ($I_{a,NP2}, D_{5-95,NP2}, D_{0-5,NP2}, D_{0-30,NP2}, f_{mid,NP2}, f'_{NP2}, \zeta_{f,NP2}$), respectively. The non-pulse-like model is thus formulated in terms of 14 parameters denoted $\alpha_{NP,i}$, $i = 1, \dots, 14$; see Table 2.

TABLE 1 Parameters $\alpha_{P,i}$ of the pulse-like model, $i = 1, \dots, 19$

Pulse	$\alpha_{P,1}$ V_p , cm/s	$\alpha_{P,2}$ T_p , s	$\alpha_{P,3}$ γ	$\alpha_{P,4}$ ν/π , rad	$\alpha_{P,5}$ $D_0 - \max_p$, s		
Residual	$\alpha_{P,6}$ $I_{a,res}$, cm/s	$\alpha_{P,7}$ $D_5 - 95_{,res}$, s	$\alpha_{P,8}$ $D_0 - 5_{,res}$, s	$\alpha_{P,9}$ $D_0 - 30_{,res}$, s	$\alpha_{P,10}$ $f_{mid,res}$, Hz	$\alpha_{P,11}$ f'_{res} , Hz/s	$\alpha_{P,12}$ $\zeta_{f,res}$
Orthogonal	$\alpha_{P,13}$ $I_{a,PO}$, cm/s	$\alpha_{P,14}$ $D_5 - 95_{,PO}$, s	$\alpha_{P,15}$ $D_0 - 5_{,PO}$, s	$\alpha_{P,16}$ $D_0 - 30_{,PO}$, s	$\alpha_{P,17}$ $f_{mid,PO}$, Hz	$\alpha_{P,18}$ f'_{PO} , Hz/s	$\alpha_{P,19}$ $\zeta_{f,PO}$

TABLE 2 Parameters $\alpha_{NP,i}$ of the non-pulse-like model, $i = 1, \dots, 14$

Major	$\alpha_{NP,1}$ $I_{a,NP1}$, cm/s	$\alpha_{NP,2}$ $D_5 - 95_{,NP1}$, s	$\alpha_{NP,3}$ $D_0 - 5_{,NP1}$, s	$\alpha_{NP,4}$ $D_0 - 30_{,NP1}$, s	$\alpha_{NP,5}$ $f_{mid,NP1}$, Hz	$\alpha_{NP,6}$ f'_{NP1} , Hz/s	$\alpha_{NP,7}$ $\zeta_{f,NP1}$
Intermediate	$\alpha_{NP,8}$ $I_{a,NP2}$, cm/s	$\alpha_{NP,9}$ $D_5 - 95_{,NP2}$, s	$\alpha_{NP,10}$ $D_0 - 5_{,NP2}$, s	$\alpha_{NP,11}$ $D_0 - 30_{,NP2}$, s	$\alpha_{NP,12}$ $f_{mid,NP2}$, Hz	$\alpha_{NP,13}$ f'_{NP2} , Hz/s	$\alpha_{NP,14}$ $\zeta_{f,NP2}$

Note that the parameters $D_0 - \max_p$, $D_0 - 5$, and $D_0 - 30$ are all measured from the nominal start time t_0 of the ground motion. In the fitting procedure, the nominal start time of a target recorded ground motion is defined as $t_{0,rec} = \min(t_{0.01,I_{a,res}}, t_{0.01,I_{a,PO}})$ for pulse-like motions and $t_{0,rec} = \min(t_{0.01,I_{a,NP1}}, t_{0.01,I_{a,NP2}})$ for non-pulse-like motions, where $t_{0.01,I_{a,comp}}$ is the time at which 0.01% of the total Arias intensity of the component is reached. Then we set $t_0, q = t_0 = t_{0,rec}$. In the simulation procedure, we usually set $t_{0,q} = t_0 = 0$. For more details, see Dabaghi and Der Kiureghian.^{4,37}

4 | EARTHQUAKE SCENARIOS AND DIRECTIVITY PARAMETERS

Characteristics of ground motions depend, to varying degrees, on the configuration of the earthquake source, on the propagation path of seismic waves traveling from the source to the site, and on the properties of the soil profile beneath the site. An earthquake scenario can be defined in terms of parameters that describe the main features of the source, path, and site. In this paper, earthquake scenarios are defined in terms of earthquake source and site characteristics that are readily available to the design engineer. These include the type of faulting F ($=0$ strike-slip faults, $=1$ reverse and reverse-oblique faults), the earthquake moment magnitude M_w , the depth Z_{TOR} to the top of the rupture plane, the closest distance R_{RUP} from the site to the fault rupture, and the shear-wave velocity V_{s30} of the top 30 m of soil at the site.

In near-fault regions, additional predictor variables are needed because ground motions also depend on the geometric configuration of the site relative to the fault rupture surface and on the direction of propagation of the rupture. Several geometric parameters have been proposed in the literature to predict and model the FD effect; see Spudich et al.⁴⁵ for a review of the directivity parameters used in the NGA-West2 directivity models. Following Iervolino and Cornell⁴⁶ and Shahi and Baker,^{16,34} the directivity parameters used in this paper are (1) the length s or width d of the portion of the rupture that propagates between the hypocenter and the site, and (2) the angle θ in a horizontal plane between the fault rupture plane and the direction between the epicenter and the site or the angle ϕ in a vertical plane between the fault rupture plane and the direction between the hypocenter and the site. Generally, parameters s and θ are used to represent directivity for strike-slip faulting, while d and ϕ are used for dip-slip faulting.² These geometric parameters are illustrated in Figure 1. For oblique-slip earthquakes, typically the parameters for dip-slip faults have been used. To better represent oblique-slip earthquakes, in this paper, the directivity parameters used for all types of faulting are (1) the larger of s and d (denoted $s_{or}d$) and (2) the corresponding angle θ or ϕ (denoted $\theta_{or}\phi$). In summary, the earthquake source and site parameters that define an earthquake scenario in this paper are $(F, M_w, Z_{TOR}, R_{RUP}, V_{s30}, s_{or}d, \theta_{or}\phi)$.

5 | DATABASE OF RECORDED NEAR-FAULT GROUND MOTIONS

A subset database of pulse-like and non-pulse-like recorded motions from PEER's NGA-West2 database (<http://peer.berkeley.edu/ngawest2/>) is selected for this study. The data consist of pairs of horizontal near-fault ground motion components from moderate to large earthquakes ($5.5 \leq M_w \leq 8.0$) recorded at sites located at $R_{RUP} < 31$ km. Only records

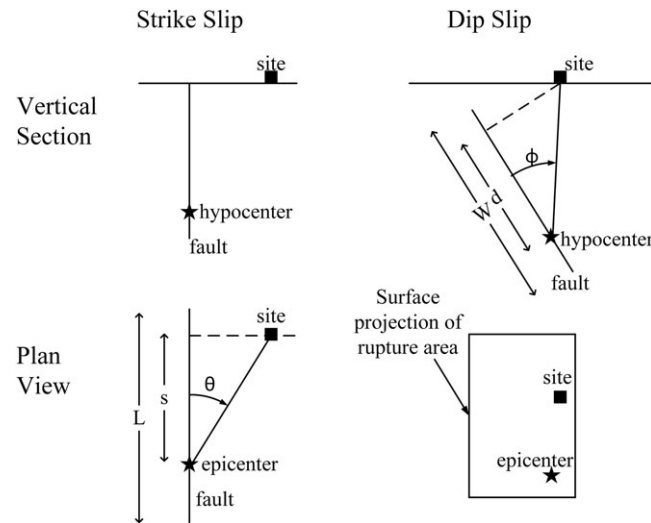


FIGURE 1 Directivity parameters (after Somerville et al²)

from shallow crustal strike-slip, reverse, or reverse-oblique earthquakes in active tectonic regions are considered. Aftershocks are excluded. Records in the NGA-West2 database have different time steps Δt . For consistency, and as discussed in more detail in Dabaghi and Der Kiureghian,³⁷ only records having time steps of $\Delta t = 0.005, 0.01, \text{ or } 0.02$ second are included. Moreover, records with $\Delta t = 0.01$ or 0.02 second are resampled to $\Delta t = 0.005$ second using a *sinc* interpolation.⁴⁷

5.1 | Pulse-like database

The pulse-like database consists of 243 recorded ground motions in the NGA-West2 database identified as pulse-like by Shahi and Baker^{16,48} (June 2012 version). To have a reasonable sample size, no limit is set on V_{s30} of the recording site. With the constraints on M_w , R_{RUP} , Δt , type of faulting, and aftershocks, the database reduces to 130 pairs of records from 27 earthquakes. The detailed list can be found in Dabaghi and Der Kiureghian³⁷; the ranges of the earthquake source and site parameters are listed in Table 3. The charts on the left side of Figure 2 show the distribution of the parameters F , M_w , R_{RUP} , and V_{s30} in the selected database.

5.2 | non-pulse-like database

The non-pulse-like database consists of recorded near-fault ground motions in the NGA-West2 database identified as non-pulse-like by Shahi and Baker.^{16,48} Since non-pulse-like records are more numerous, in addition to the constraints on M_w , R_{RUP} , Δt , etc, we exclude records at soft sites with $V_{s30} < 360$ m/s. The resulting non-pulse-like database consists of 311 pairs of records from 44 earthquakes. A detailed list can be found in Dabaghi and Der Kiureghian³⁷; the ranges of the earthquake source and site parameters are listed in Table 4. The charts on the right side of Figure 2 show the distribution of the parameters F , M_w , R_{RUP} , and V_{s30} in the selected database.

5.3 | Identification of model parameters

Sample “observations” of the model parameters are obtained by fitting each ground motion model to the corresponding database of recorded near-fault ground motions. Each record in the pulse-like database is rotated into the direction containing the largest pulse amplitude $a_{PP}(t)$ and the corresponding orthogonal horizontal direction $a_{PO}(t)$. Moreover, the

TABLE 3 Ranges of earthquake source and site parameters for records in the pulse-like database

	M_w	Z_{TOR} , km	R_{RUP} , km	V_{s30} , m/s	s or d , km	θ or ϕ , °
Min	5.74	0	0.07	139	4.97	0.1
Max	7.90	5.92	30.49	2016	101.51	67.4

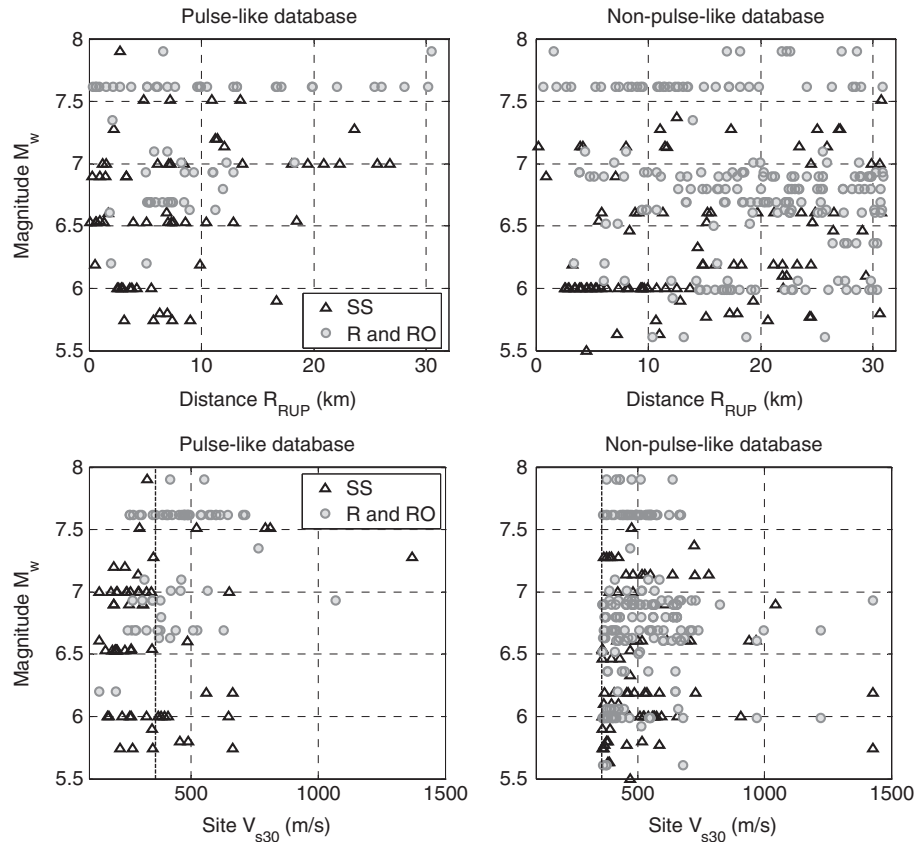


FIGURE 2 Distribution of records in the pulse-like (left) and non-pulse-like (right) databases with respect to type-of-faulting, moment magnitude, source-to-site distance, and shear-wave velocity at the site

TABLE 4 Ranges of earthquake source and site parameters for records in the non-pulse-like database

	M_w	Z_{TOR} , km	R_{RUP} , km	V_{s30} , m/s	s or d , km	θ or ϕ , °
Min	5.50	0	0.21	361	1.20	0.15
Max	7.90	14.50	30.9	1428	135	84.4

velocity pulse $v_{pul}(t)$ is extracted from the ground motion component in the direction of the largest pulse using Baker's algorithm,⁴¹ and the corresponding residual motion $a_{res}(t)$ is calculated. Similarly, each record in the non-pulse-like database is rotated into the major and intermediate "principal" components, $a_{NP1}(t)$ and $a_{NP2}(t)$. Fitting is achieved by matching selected intensity, duration, and frequency content characteristics of the model to those of each recorded motion. The procedure is described and illustrated in Dabaghi and Der Kiureghian.^{4,37} A complete list of the identified model parameters for the records in the selected databases is given in Dabaghi and Der Kiureghian.³⁷ Note that the values " $t_{max,p}$ measured from t_0 " in Dabaghi and Der Kiureghian³⁷ correspond to $D_0 - max,p$ in this paper. Also see Dabaghi and Der Kiureghian³⁷ for more details on how the components are rotated, the directivity pulse and residual motion separated, and the time series resampled to $\Delta t = 0.005$ second.

6 | DEVELOPMENT OF EMPIRICAL PREDICTIVE EQUATIONS FOR PARAMETERS OF STOCHASTIC MODEL

Using the samples of fitted model parameters, predictive models are developed for the pulse-like and non-pulse-like model parameters in a transformed normal space. They include (1) predictive mean equations in terms of the predictor variables (F , M_w , Z_{TOR} , R_{RUP} , V_{s30} , s or d , and θ or ϕ) that describe the earthquake source and site characteristics, (2) estimates of the standard deviations of the transformed model parameters, and (3) estimates of the statistical correlations between the model parameters.

6.1 | Transformation of model parameters to the normal space

First, all the model parameters $\alpha_{P,i}$, $i = 1, \dots, 19$, and $\alpha_{NP,i}$, $i = 1, \dots, 14$, are transformed to the normal space to satisfy the normality assumption in the subsequent development of regression models. The transformed pulse-like and non-pulse-like model parameters are denoted $z_{P,i}$, $i = 1, \dots, 19$, and $z_{NP,i}$, $i = 1, \dots, 14$, respectively. The model parameters can be classified into 4 categories: (1) intensity parameters (V_p and I_a), (2) period and frequency parameters (T_p and f_{mid}), (3) time and duration parameters ($D_0 - max,p$, $D_0 - 5$, $D_0 - 30$, and $D_5 - 95$), and (4) “other” parameters (γ , ν , f' , and ζ_f) that are difficult to relate to physical ground motion characteristics and are likely to be least important for structural response. Ground motion intensity, frequency, and time and duration parameters can be reasonably assumed to follow a lognormal distribution (see, eg, Abrahamson⁴⁹ and Jayaram and Baker⁵⁰ for intensity measures; Bray and Rodriguez-Marek¹⁵ and Rathje et al⁵¹ for frequency parameters; and Kempton and Stewart⁵² and Bommer⁵³ for duration parameters). These parameters are transformed to the normal space by taking their natural logarithms:

$$z_{P,i} = \ln \alpha_{P,i} \quad i = 1, 2, 5, 6, 7, 8, 9, 10, 13, 14, 15, 16, 17, \quad (6)$$

$$z_{NP,i} = \ln \alpha_{NP,i} \quad i = 1, 2, 3, 4, 5, 8, 9, 10, 11, 12. \quad (7)$$

Because the remaining model parameters (γ , ν , f' , and ζ_f) do not follow a lognormal distribution, the procedure described by Rezaeian and Der Kiureghian^{44,54} is used: A marginal probability distribution $F_{\alpha_{P,i}}(\alpha_{P,i})$ or $F_{\alpha_{NP,i}}(\alpha_{NP,i})$ is fitted to the sample data of each parameter. The parameter is then transformed to the standard normal space by use of the rules

$$z_{P,i} = \Phi^{-1}[F_{\alpha_{P,i}}(\alpha_{P,i})], \quad i = 3, 4, 11, 12, 18, 19, \quad (8)$$

$$z_{NP,i} = \Phi^{-1}[F_{\alpha_{NP,i}}(\alpha_{NP,i})], \quad i = 6, 7, 13, 14, \quad (9)$$

where $\Phi^{-1}[\cdot]$ denotes the inverse of the standard normal cumulative probability distribution function. Table 5 lists the fitted marginal distributions, their selected bounds, and fitted parameter values. See Dabaghi and Der Kiureghian³⁷ for definitions of distribution parameters.

6.2 | Regression analysis

Next, the transformed data are regressed against the variables (F , M_w , Z_{TOR} , R_{RUP} , V_{s30} , s_{ord} , $\theta_{or}\phi$). In all cases, the directivity parameter $\theta_{or}\phi$ was found not to be a good predictor and was removed from the list.

Random effects regression is used to properly account for the statistical dependence of multiple observations from the same earthquake and to prevent earthquakes with large numbers of records from biasing the results. The total regression error is subdivided into an inter-event term η_i and an intra-event term ϵ_i , where subscript i denotes the model parameter of interest. These error terms are assumed to be independent, normally distributed random variables with zero means and variances τ_i^2 and ϕ_i^2 , respectively.^{55,56} The variance of the total regression error ($\eta_i + \epsilon_i$) is given by $\sigma_{T,i}^2 = \tau_i^2 + \phi_i^2$. The regression formulae for the transformed model parameters have the forms

$$z_{P,i} = g_{P,i}(F, M_w, Z_{TOR}, R_{RUP}, V_{s30}, s_{ord}) + \eta_{P,i} + \epsilon_{P,i} \quad i = 1, \dots, 19, \quad (10)$$

$$z_{NP,i} = g_{NP,i}(F, M_w, Z_{TOR}, R_{RUP}, V_{s30}, s_{ord}) + \eta_{NP,i} + \epsilon_{NP,i} \quad i = 1, \dots, 14, \quad (11)$$

TABLE 5 Marginal distributions fitted to parameters γ , ν , f' , and ζ_f

Parameter	Unit	Fitted Distribution	Selected Lower Bound	Selected Upper Bound	Fitted Distribution Parameters
γ	–	Beta	2.0	3.2	$\alpha = 1.30$, $\beta = 3.97$
ν/π	π , rad	Uniform	0	2	
f'	Hz/s	Two-sided exponential	–3.5	1.5	$\alpha = 6.4$, $\beta = 14.3$, $c = 4.42$
$\ln \zeta_f$	–	Beta	$\ln 0.009$	$\ln 1$	$\alpha = 5.34$, $\beta = 3.83$

where $g_{P,i}(\cdot) = E[z_{P,i}] = \sum_j \beta_{P,ij} X_j$ and $g_{NP,i}(\cdot) = E[z_{NP,i}] = \sum_j \beta_{NP,ij} X_j$ are the linear predictive mean equations for the pulse-like and non-pulse-like model parameters, respectively. We use linear predictive equations to avoid the more difficult task of nonlinear regression analysis.

For consistency with seismological theory, the functional form of the predictive equation of any transformed model parameter z is initially constructed as the sum of terms that represent the source (magnitude and type of faulting), the path (geometric attenuation term), the site (shallow site response term), and the directivity effect. The same general form and regression terms X_j are selected for both the pulse-like and non-pulse-like model parameters:

$$E[z] = \sum_j \beta_j X_j \\ = \beta_0 + \beta_1 M_w + \beta_2 (M_w - 6.5) \mathbb{I}(M_w > 6.5) + \beta_3 F f_{fl,Z} + (\beta_4 + \beta_5 M_w) \ln \left(\sqrt{R_{RUP}^2 + h^2} \right) + \beta_6 \ln \hat{V}_{s30} + \beta_7 s_{or} d. \quad (12)$$

In the above, $\mathbb{I}(\cdot)$ is the indicator function ($=1$ if the term inside brackets is true, $=0$ otherwise), $f_{fl,Z} = Z_{TOR}$ if $Z_{TOR} < 1$ km and $f_{fl,Z} = 1$ if $Z_{TOR} \geq 1$ km, h is the effective focal depth, and $\hat{V}_{s30} = \min(V_{s30}, 1100 \text{ m/s})$. This general form is adapted from existing GMPEs developed for intensity measures by Campbell and Bozorgnia,^{57,58} to which we add a directivity term. To avoid nonlinearity in the regression equation, we set $h = 6$ km before performing regression analysis. The directivity variable $s_{or}d$ is only considered in the predictive relations for the parameters of the pulse-like model; therefore, we set $\beta_{NP,i7} = 0$.

Equation (12) is used as a starting point for the predictive equations of all model parameters. However, not all terms are included in the final versions; only terms having explanatory power are retained. In fact, the simplest model that minimizes the variance of the error terms is preferred over more complex models. Equation (12) is thus adapted to the data. For instance, we find that only the magnitude and distance terms provide explanatory power for parameters (γ , ν , f' , and ζ_j). Therefore, we set $\beta_2 = \beta_3 = \beta_5 = \beta_6 = \beta_7 = 0$ for these parameters. Moreover, some terms are removed

TABLE 6 Estimates of regression coefficients and error standard deviations for parameters of the pulse-like model ($\mathbf{z}_{P,i}$)

i	$\alpha_{P,i}$	$\hat{\beta}_{P,i0}$	$\hat{\beta}_{P,i1}$	$\hat{\beta}_{P,i2}$	$\hat{\beta}_{P,i3}$	$\hat{\beta}_{P,i4}$	$\hat{\beta}_{P,i5}$	$\hat{\beta}_{P,i6}$	$\hat{\beta}_{P,i7}$	$\hat{\sigma}_{0,i}$	$\hat{\phi}_i$	$\hat{\tau}_i$	$\hat{\sigma}_{T,i}$
1	V_p	1.699	0.608	-0.608*	0.183	-0.576	-	-0.094	0.007	0.463	0.385	0	0.385
6	$I_{a,res}$	-2.116	1.474	-1.378	0.337	-1.073	-	-	-	0.904	0.592	0.510	0.781
13	$I_{a,PO}$	-0.263	1.131	-1.170	0.404	-1.652	0.105	-	-	0.884	0.669	0.331	0.747
2	T_p	-2.479	0.670	-	-0.264	-	-	-0.233	0.008	0.869	0.359	0.457	0.581
10	$f_{mid,res}$	0.967	-0.111	-	-	-	-	0.183	-	0.422	0.385	0.142	0.410
17	$f_{mid,PO}$	0.434	-0.125	-	-	-	-	0.302	-	0.459	0.405	0.171	0.440
5**	$D_0 - max,p$	-4.249	0.852	-	-0.380	0.390	-	-0.088	-	0.842	0.272	0.382	0.469
7	$D_5 - 95,res$	-0.381	0.733	-	-0.163	0.217	-	-0.427	-	0.589	0.279	0.247	0.372
8	$D_0 - 5,res$	-5.563	0.905	-	-0.282	0.385	-	-	-	0.779	0.307	0.318	0.442
9	$D_0 - 30,res$	-4.777	0.880	-	-0.339	0.311	-	-	-	0.764	0.241	0.311	0.394
14	$D_5 - 95,PO$	-0.516	0.754	-	-0.122	0.192	-	-0.424	-	0.630	0.292	0.277	0.402
15	$D_0 - 5,PO$	-5.772	0.923	-	-0.238	0.403	-	-	-	0.772	0.325	0.328	0.461
16	$D_0 - 30,PO$	-5.016	0.905	-	-0.328	0.327	-	-	-	0.764	0.233	0.334	0.408
3	γ	-	-	-	-	-	-	-	-	1.002	1.002	0	1.002
4	ν	-	-	-	-	-	-	-	-	0.928	0.928	0	0.928
11	f'_{res}	-2.166	0.322	-	-	-	-	-	-	0.838	0.820	0	0.820
12	ζ_{res}	-1.707	0.433	-	-	-0.413	-	-	-	1.118	1.096	0	1.096
18	f'_{PO}	-2.875	0.416	-	-	-	-	-	-	0.857	0.825	0	0.825
19	ζ_{PO}	-1.868	0.457	-	-	-0.501	-	-	-	0.996	0.962	0	0.962

* $\beta_2 = -\beta_1$ is imposed to prevent oversaturation, ie, a decrease in V_p with increasing magnitude.

**In Dabaghi and Der Kiureghian,³⁷ $D_0 - max,p$ was denoted $t_{max,p}$ and measured from t_0 .

from Equation (12) for consistency with existing GMPEs developed for similar parameters. For example, following Bommer et al,⁵³ we set $\beta_2 = 0$ for the time and duration parameters. Note that here, we set $h = 6$ km while $h = 2.5$ km was used in Bommer et al.⁵³

The regression coefficients $\beta_{P,ij}$ and $\beta_{NP,ij}$ are solved for numerically following the method described in Rezaeian and Der Kiureghian.^{44,54} We use the statistical F-test to evaluate whether τ_i is statistically different from zero, ie, whether the random effect should be included or not. If the F-test is passed with τ_i at least 82% confidence, we include the random effect. In most cases where the random effect is included, the F-test is passed with greater than 95% confidence. In the cases where the data do not support the use of the random effects regression model, we set $\tau_i = 0$ and use regular regression analysis. The selected combinations of the regression terms are listed in Tables 6 and 7 for the parameters of the pulse-like and non-pulse-like models, respectively. A dash indicates that a regression term is not included in the final regression form. Listed in these tables are the estimates of the regression coefficients $\beta_{P,ij}$ and $\beta_{NP,ij}$ and the standard deviations τ_i , ϕ_i , and $\sigma_{T,i}$ of the inter-event, intra-event, and total error terms, respectively. When the random effect is not included, only $\sigma_{T,i}$ is listed. The initial sample standard deviation $\sigma_{0,i}$ of the data is also given for reference. A large decrease in the standard deviation from $\sigma_{0,i}$ to $\sigma_{T,i}$ indicates that the selected regression equation has a significant explanatory power. Because of the limited size of the data and complexity of the ground motion phenomenon, we are able to achieve only small to moderate reductions in the total standard deviations. As more data become available, the functional forms and coefficients of the regression equations can be updated, and error standard deviations are likely to decrease. After selecting the final regression equation, the normality assumption is checked by examining the regression residuals. We also use a variant of cross-validation to ensure that the selected models do not overfit the data; we randomly remove 10% of the data points for each model parameter and rerun the regressions. The estimated regression coefficient values change only slightly, confirming robustness of the selected regression formulae. These and other details of the analysis are reported in Dabaghi and Der Kiureghian.³⁷ Also reported there are the lower and upper bounds of the 95% confidence intervals of the estimates of the regression coefficients, as well as the importance factor of each predictive term for each model parameter. The importance factors indicate that terms related to magnitude and distance scaling tend to be the most important for many of the parameters of our model.³⁷

6.3 | Analysis of regression results

The trends observed in Tables 6 and 7 between the model parameters and the earthquake source and site characteristics make sense overall. They are generally as expected based on seismological principles and consistent with prior observations and existing GMPEs (see Dabaghi and Der Kiureghian³⁷ for a comparison with existing GMPEs). The advantage of

TABLE 7 Estimates of regression coefficients and error standard deviations for parameters of the non-pulse-like model ($\mathbf{z}_{NP,i}$)

i	$\alpha_{NP,i}$	$\hat{\beta}_{NP,i0}$	$\hat{\beta}_{NP,i1}$	$\hat{\beta}_{NP,i2}$	$\hat{\beta}_{NP,i3}$	$\hat{\beta}_{NP,i4}$	$\hat{\beta}_{NP,i5}$	$\hat{\beta}_{NP,i6}$	$\hat{\beta}_{NP,i7}$	$\hat{\sigma}_{0,i}$	$\hat{\phi}_i$	$\hat{\tau}_i$	$\hat{\sigma}_{T,i}$
1	$I_{a,NP1}$	8.097	1.006	-1.393	0.435	-4.859	0.473	-0.863	-	1.432	0.903	0.541	1.053
8	$I_{a,NP2}$	7.307	0.999	-1.331	0.443	-4.953	0.491	-0.835	-	1.418	0.819	0.622	1.028
5	$f_{mid,NP1}$	0.247	-0.149	-	-	-	-	0.377	-	0.480	0.397	0.207	0.448
12	$f_{mid,NP2}$	0.425	-0.181	-	-	-	-	0.402	-	0.441	0.353	0.189	0.400
2	$D_5 - 95_{NP1}$	-1.035	0.769	-	-0.378	0.412	-	-0.424	-	0.656	0.378	0.125	0.398
3	$D_0 - 5_{NP1}$	-4.727	0.710	-	-0.124	0.471	-	-	-	0.663	0.355	0.287	0.457
4	$D_0 - 30_{NP1}$	-4.444	0.798	-	-0.231	0.345	-	-	-	0.635	0.288	0.104	0.306
9	$D_5 - 95_{NP2}$	-0.404	0.672	-	-0.330	0.335	-	-0.367	-	0.590	0.334	0.172	0.376
10	$D_0 - 5_{NP2}$	-4.798	0.709	-	-0.076	0.473	-	-	-	0.662	0.356	0.289	0.458
11	$D_0 - 30_{NP2}$	-4.350	0.785	-	-0.222	0.325	-	-	-	0.610	0.278	0.096	0.294
6	f'_{NP1}	-1.443	0.223	-	-	-	-	-	-	0.949	0.941	0	0.941
7	ζ_{NP1}	-0.380	0.159	-	-	-0.298	-	-	-	1.018	1.008	0	1.008
13	f'_{NP2}	-2.979	0.420	-	-	-	-	-	-	0.866	0.832	0	0.832
14	ζ_{NP2}	-0.704	0.161	-	-	-0.146	-	-	-	0.892	0.888	0	0.888

our relations is that they make the crucial distinction between pulse-like and non-pulse-like ground motions. Some of the trends are discussed next.

V_p is positively related to $s_{or}d$ ($\beta_7 > 0$), in accordance with the FD effect. The type of faulting ($\beta_3 X_3$) is found to make little contribution to the overall predictive equation; it is retained here for comparison with existing GMPEs for intensity measures.^{57,58} Moreover, the random effect is not found to be statistically significant for V_p , indicating that the amplitudes of velocity pulses arising from the same event but observed at different sites are not strongly correlated. T_p tends to increase with the magnitude ($\beta_1 > 0$) and decrease with site stiffness ($\beta_6 < 0$), which is as expected and agrees with previous observations, even though T_p is not uniquely defined in the literature.^{15,19,22,28,32,41} It appears that strike-slip earthquakes result in pulses with periods longer than reverse earthquakes ($\beta_3 < 0$). Moreover, as $s_{or}d$ increases, T_p tends to increase ($\beta_7 > 0$), which is as expected since wave periods tend to lengthen with increasing rupture length and duration.

For the 2 horizontal components of both pulse-like and non-pulse-like ground motions, f_{mid} decreases with magnitude ($\beta_1 < 0$) and increases with site stiffness ($\beta_6 > 0$). All the time and duration parameters tend to increase with magnitude ($\beta_1 > 0$) and distance ($\beta_4 > 0$) and are smaller for buried reverse fault ruptures ($\beta_3 < 0$). Soil stiffness has a statistically significant effect on $D_0 - max,p$, which defines the time position of the pulse within the record, and on the effective duration parameter $D_5 - 95$, but not on the remaining time parameters; $D_0 - max,p$ and $D_5 - 95$ tend to decrease with soil stiffness ($\beta_6 < 0$). These trends are as expected. Moreover and also as expected, effective durations of pulse-like motions tend to be shorter than those of non-pulse-like motions.

The predictive relations for the “other” parameters are only able to explain a small portion of the observed variability, as illustrated by the small decrease in variances from $\sigma_{0,i}^2$ to $\sigma_{T,i}^2$. No viable predictive relations were found for $z_{P,3}$ or $z_{P,4}$ (corresponding to γ and ν). Therefore, consistent with their marginal distributions, $z_{P,3}$ and $z_{P,4}$ are simply assumed to come from standard normal distributions. The values of $\sigma_{T,i}$ ($=\sigma_{0,i}$) for these parameters are slightly different from 1 since they are the sample standard deviations. The trends followed by the filter parameters f' and ζ are generally similar to those documented in Rezaeian and Der Kiureghian^{44,54} for far-field motions.

6.4 | Correlation analysis

For a given earthquake scenario, the parameters $z_{P,i}$ and therefore $\alpha_{P,i}$ of the pulse-like model are correlated. Similarly, the parameters $z_{NP,i}$ and therefore $\alpha_{NP,i}$ of the non-pulse-like model are correlated. The correlation coefficients $\rho_{P,ij}$ between pairs of the parameters $z_{P,i}$, $i = 1, \dots, 19$, are estimated as the correlations between the corresponding total regression residuals ($\widehat{\eta}_{P,i} + \widehat{\epsilon}_{P,i}$). Similarly, the correlation coefficients $\rho_{NP,ij}$ between pairs of the parameters $z_{NP,i}$, $i = 1, \dots, 14$, are estimated as the correlations between the corresponding total regression residuals ($\widehat{\eta}_{NP,i} + \widehat{\epsilon}_{NP,i}$). The estimated correlation coefficients $\rho_{P,ij}$ and $\rho_{NP,ij}$ (rounded to 2 significant figures) are listed in Tables 8 and 9, respectively. Correlation values larger than 0.3 in absolute value are highlighted.

These correlations describe the statistical dependencies between the model parameters for given values of the earthquake and site characteristics. As expected, larger positive correlations are generally observed for the same parameters of the residual and orthogonal motions (0.42 to 0.93) and of the major and intermediate components (0.65 to 0.95), and for parameters of the same category. We find (mild) negative correlation (−0.2) between $z_{P,1}$ and $z_{P,2}$, which correspond to V_p and T_p . We also find positive correlation (0.4) between V_p and the I_a parameters. Thus, a pulse-like motion with a large pulse amplitude tends to have high intensity residual and orthogonal motions. We also find positive correlations between T_p and $D_0 - max,p$ (0.4) and with time parameters $D_0 - 5$ and $D_0 - 30$ (0.3 to 0.4, respectively). Additionally, the time parameters $D_0 - max,p$, $D_5 - 95$, $D_0 - 5$, and $D_0 - 30$ are all strongly positively correlated with each other (0.7 to 0.9), as expected. Concerning the filter parameters, mild negative correlations (−0.2 and −0.4) are found between f_{mid} and f' of the residual and orthogonal motions, respectively. Practically no correlation is found between the frequency contents of the pulse, residual, and orthogonal motions, namely, T_p and f_{mid} . The correlations between the parameters of the major and intermediate “principal” components of the non-pulse-like model are almost identical to the correlations between the parameters of the residual and orthogonal motions of the pulse-like model.

7 | PROBABILITY OF OCCURRENCE OF A PULSE

For a complete representation of the near-fault ground motion for a given earthquake scenario, 2 additional pieces of information are needed. The first piece is the probability of the ground motion being pulse-like at the site, which should

TABLE 8 Estimated correlation matrix of regression residuals for the parameters of the pulse-like model $z_{p,i}$ (for legibility, subscript P is dropped; moderate to large correlations are highlighted)

$z_{p,i}$	z_1	z_2	z_3	z_4	z_5	z_6	z_7	z_8	z_9	z_{10}	z_{11}	z_{12}	z_{13}	z_{14}	z_{15}	z_{16}	z_{17}	z_{18}	z_{19}
z_1	1	-0.18	-0.02	0.17	0.19	0.45	0.04	0.03	0.12	-0.38	0.06	0.16	0.41	-0.04	0.02	0.04	-0.28	0.11	0.05
z_2		1	0.18	0.00	0.43	-0.08	0.10	0.31	0.37	0.05	0.02	0.18	-0.10	0.14	0.30	0.37	0.04	-0.07	0.24
z_3			1	-0.19	0.24	0.18	0.11	0.15	0.24	-0.11	0.05	0.06	0.07	0.13	0.09	0.21	-0.07	0.02	0.12
z_4				1	0.12	-0.08	0.09	0.07	0.07	-0.13	-0.09	0.03	-0.02	-0.02	0.07	0.07	-0.15	0.10	-0.04
z_5					1	0.06	0.16	0.73	0.79	-0.03	-0.15	0.13	0.02	0.19	0.68	0.75	0.01	-0.17	0.19
z_6						1	-0.02	0.06	0.09	0.08	0.10	0.03	0.84	0.02	0.01	0.08	0.13	0.08	0.05
z_7							1	0.06	0.25	-0.02	-0.22	0.05	0.04	0.76	0.04	0.21	-0.08	-0.03	-0.03
z_8								1	0.86	0.01	-0.05	0.20	0.02	0.15	0.93	0.85	0.02	0.00	0.24
z_9									1	0.03	-0.06	0.20	0.10	0.26	0.80	0.91	0.04	-0.01	0.23
z_{10}										1	-0.24	0.11	0.17	-0.05	0.05	0.11	0.86	-0.29	0.16
z_{11}											1	0.11	-0.01	-0.05	-0.06	-0.09	-0.09	0.42	0.24
z_{12}												1	-0.03	0.09	0.16	0.26	0.28	-0.18	0.79
z_{13}													1	-0.17	0.01	0.06	0.10	0.17	-0.04
z_{14}														1	0.06	0.24	0.01	-0.13	0.09
z_{15}															1	0.84	0.03	0.04	0.18
z_{16}																1	0.1	-0.08	0.28
z_{17}																	1	-0.43	0.26
z_{18}																		1	-0.18
z_{19}																			1

Symmetric

TABLE 9 Estimated correlation matrix of regression residuals for the parameters of the non-pulse-like model $z_{NP,i}$ (for legibility, subscript NP is dropped; moderate to large correlations are highlighted)

$z_{NP,i}$	z_1	z_2	z_3	z_4	z_5	z_6	z_7	z_8	z_9	z_{10}	z_{11}	z_{12}	z_{13}	z_{14}
z_1	1	-0.18	0.09	0.10	0.01	0.20	-0.15	0.95	-0.08	0.05	0.10	0.09	0.10	-0.12
z_2		1	0.09	0.31	-0.02	-0.15	0.09	-0.08	0.85	0.10	0.29	-0.06	-0.02	0.11
z_3			1	0.81	-0.23	0.00	-0.08	0.06	0.14	0.91	0.79	-0.19	-0.02	-0.09
z_4				1	-0.16	-0.09	-0.02	0.13	0.29	0.75	0.91	-0.15	-0.06	-0.05
z_5					1	-0.19	-0.16	0.07	-0.08	-0.17	-0.17	0.90	-0.08	0.00
z_6						1	-0.09	0.15	-0.03	0.00	-0.09	-0.09	0.65	-0.16
z_7							1	-0.11	0.06	-0.07	-0.02	-0.09	-0.11	0.76
z_8								1	-0.07	0.05	0.12	0.10	0.14	-0.11
z_9									1	0.08	0.29	-0.09	-0.05	0.10
z_{10}										1	0.79	-0.18	0.01	-0.07
z_{11}			Symmetric								1	-0.17	-0.08	-0.03
z_{12}												1	-0.18	0.01
z_{13}													1	-0.11
z_{14}														1

reflect the proportion of pulse-like and non-pulse-like synthetic motions generated for the site. The second is the ground motion directionality, which is described in the next section.

We use the empirical model developed by Shahi and Baker³⁴ to compute the probability of observing a pulse at the site:

$$\Pr[\text{pulse-like}|F, R_{RUP}, s_{or}d, \theta_{or}\phi] = \frac{1}{1 + \exp(0.457 + 0.126R_{RUP} - 0.244\sqrt{s_{or}d} + 0.013\theta_{or}\phi)}, \quad \text{if } F = 0$$

$$\Pr[\text{pulse-like}|F, R_{RUP}, s_{or}d, \theta_{or}\phi] = \frac{1}{1 + \exp(0.304 + 0.072R_{RUP} - 0.208\sqrt{s_{or}d} + 0.021\theta_{or}\phi)}, \quad \text{if } F = 1 \quad (13)$$

where R_{RUP} and $s_{or}d$ are in kilometers and $\theta_{or}\phi$ is in degrees. While an earlier version of this model¹⁶ was used in Dabaghi and Der Kiureghian,³⁷ the more recent version is preferred here because it tends to predict lower and more realistic pulse probabilities for the distances of interest.

8 | GROUND MOTION DIRECTIONALITY

A model of the directionality of the motion is needed to provide the orientation of the ground motion components relative to the fault strike. Thus, we develop empirical predictive models of (1) the angle α_p between the direction of the largest pulse and the strike of the fault for pulse-like motions and (2) the angle α_{NP1} between the major “principal” direction and the strike of the fault for non-pulse-like motions. For each record in the pulse-like database, α_p is documented in Shahi.⁴⁸ We fit a simple trapezoidal probability density function to the data. By least-squares fitting of the corresponding cumulative distribution function $F_{\alpha_p}(\alpha_p)$ to the empirical cumulative distribution function of α_p , together with the linear constraints $F_{\alpha_p}(\alpha_p = 0) = 0$ and $F_{\alpha_p}(\alpha_p = 90) = 1$, we obtain the probability density function

$$f_{\alpha_p}(\alpha_p) = 0.0014 + 2.155 \cdot 10^{-4} \alpha_p, \quad 0^\circ \leq \alpha_p \leq 90^\circ. \quad (14)$$

For each record in the non-pulse-like database, we compute the angle α_{NP1} . The obtained empirical distribution appears to be nearly uniform. Hence, we use a uniform distribution for α_{NP1} over the interval $0^\circ \leq \alpha_{NP1} \leq 90^\circ$.

9 | SIMULATION OF NEAR-FAULT GROUND MOTIONS FOR SPECIFIED EARTHQUAKE SOURCE AND SITE CHARACTERISTICS

To generate synthetic near-fault ground motions for specified earthquake source and site characteristics, the necessary input parameters are $(F, M_w, Z_{TOR}, R_{RUP}, V_{s30}, s_{or}d, \theta_{or}\phi)$, which are typically available to the design engineer. The pulse probability model in (13) is used to generate the proportion of pulse-like and non-pulse-like ground motions. The predictive equations (11) and (12) and the estimated standard deviations and correlations between the model parameters are used to generate random realizations of the parameters of the pulse-like and non-pulse-like models. In turn, and as described in Dabaghi and Der Kiureghian,⁴ the simulated model parameters are used in the corresponding stochastic models of pulse-like and non-pulse-like motions to generate random realizations of synthetic near-fault ground motions for the given earthquake scenario. The pulse-like and non-pulse-like directionality models described in Section 8 are used to generate the orientation of the simulated components relative to the strike of the fault.

More specifically, to simulate one realization of a pair of orthogonal horizontal components of a near-fault ground motion for a specified earthquake scenario $(F, M_w, Z_{TOR}, R_{RUP}, V_{s30}, s_{or}d, \theta_{or}\phi)$, we proceed as follows.

9.1 | Step 1: Simulate the pulse-like or non-pulse-like nature of the ground motion

Given $(F, R_{RUP}, s_{or}d, \theta_{or}\phi)$, compute $\text{Pr}[\text{pulse} - \text{like} | F, R_{RUP}, s_{or}d, \theta_{or}\phi]$ in (13). Generate a random number uniformly distributed between 0 and 1. If the sampled number is less than or equal to $\text{Pr}[\text{pulse} - \text{like} | F, R_{RUP}, s_{or}d, \theta_{or}\phi]$, a pulse-like motion should be generated; otherwise, a non-pulse-like motion should be generated.

9.2 | Step 2: Simulate model parameters and orientation of the ground motion

For a pulse-like motion,

1. given $(F, M_w, Z_{TOR}, R_{RUP}, V_{s30}, s_{or}d)$, compute the conditional mean values of the transformed pulse-like model parameters $z_{P,1}, \dots, z_{P,19}$ by use of the predictive equations in (12) with the regression coefficients listed in Table 6;
2. add to the computed mean values simulated values of the corresponding total errors $(\eta_{P,i} + \epsilon_{P,i})$, $i = 1, \dots, 19$, generated as correlated normal random variables with zero means, variances $\tau_i^2 + \sigma_i^2$ as listed in Table 6, and correlation coefficients as listed in Table 8;
3. transform generated $z_{P,i}$ values back to the original space according to the inverses of the relations in (6) and (8);
4. use the computed residual motion parameters $(I_{a,res}, D_{5-95,res}, D_{0-5,res}, D_{0-30,res})$ and orthogonal motion parameters $(I_{a,PO}, D_{5-95,PO}, D_{0-5,PO}, D_{0-30,PO})$ to back-calculate the modulating function parameters $(\alpha_{res}, \beta_{res}, c_{res}, t_{max,q,res})$ and $(\alpha_{PO}, \beta_{PO}, c_{PO}, t_{max,q,PO})$, respectively; see Dabaghi and Der Kiureghian⁴ for details;
5. generate the orientation angle α_P of the largest pulse relative to the strike of the fault by randomly sampling a number between 0° and 90° according to the probability distribution in (14).

For a non-pulse-like motion,

1. given $(F, M_w, Z_{TOR}, R_{RUP}, V_{s30})$, compute the conditional mean values of the transformed non-pulse-like model parameters $z_{NP,1}, \dots, z_{NP,14}$, by use of the predictive equations in (12) with the regression coefficients listed in Table 7;
2. add to the computed mean values simulated values of the corresponding total errors $(\eta_{NP,i} + \epsilon_{NP,i})$, $i = 1, \dots, 14$, generated as correlated normal random variables with zero means, variances $\tau_i^2 + \sigma_i^2$ as listed in Table 7, and correlation coefficients as listed in Table 9;
3. transform generated $z_{NP,i}$ values back to the original space according to the inverses of the relations in (7) and (9);
4. use the computed parameters $(I_{a,NP1}, D_{5-95,NP1}, D_{0-5,NP1}, D_{0-30,NP1})$ and $(I_{a,NP2}, D_{5-95,NP2}, D_{0-5,NP2}, D_{0-30,NP2})$ of the major and intermediate “principal” components to back-calculate the modulating function parameters $(\alpha_{NP1}, \beta_{NP1}, c_{NP1}, t_{max,q,NP1})$ and $(\alpha_{NP2}, \beta_{NP2}, c_{NP2}, t_{max,q,NP2})$, respectively; see Dabaghi and Der Kiureghian⁴ for details;
5. generate the orientation angle α_{NP1} of the major “principal” component relative to the strike of the fault by uniformly sampling a number between 0° and 90° .

9.3 | Step 3: Simulate synthetic ground motion components

The procedure described in Dabaghi and Der Kiureghian⁴ is used to generate and postprocess a synthetic pair of near-fault ground motion components for the simulated set of correlated model parameters. The postprocessing used is summarized in the following section. As pointed out in Dabaghi and Der Kiureghian,⁴ there is no guarantee that the parameters ($I_a, MFW, D_0 - 5, MFW, D_0 - 30, MFW, D_0 - 95, MFW$) of a synthetic acceleration time series generated using target simulated modulating function parameters ($I_a, D_0 - 5, D_0 - 30, D_0 - 95$) will actually match the target parameters. Therefore, as described in Dabaghi and Der Kiureghian,⁴ a uniform scaling is applied after postprocessing to each synthetic component so that the scaled synthetic acceleration $a_{MFW}^*(t)$ has total Arias intensity that matches the target Arias intensity parameter I_a of the component in question. Matching of the simulated parameter values ($D_0 - 5, D_0 - 30, D_0 - 95$) can only be guaranteed in an average sense. Since the synthetic motions are being generated for a hypothetical earthquake scenario, we usually set $t_{0,q} = t_0 = 0$.

If the simulated motion is pulse-like, the parameters ($V_p, T_p, \gamma, \nu, D_0 - max_p$) of the mMP pulse model, ($\alpha_{res}, \beta_{res}, c_{res}, t_{max,q,res}, f_{mid,res}, f'_{res}, \zeta_{f,res}$) of the residual motion, and ($\alpha_{PO}, \beta_{PO}, c_{PO}, t_{max,q,PO}, f_{mid,PO}, f'_{PO}, \zeta_{f,PO}$) of the orthogonal motion are used to generate the horizontal components of a pulse-like near-fault ground motion in the direction α_p of the largest pulse and in the orthogonal direction. The classification method developed by Shahi and Baker¹⁶ is then applied to the synthetic ground motion to check if the simulated pulse is indeed identified as a pulse by the algorithm. If the synthetic ground motion is classified as non-pulse-like by the algorithm, which occurs on a few occasions, the synthetic motion is discarded, and Step 3 is repeated.

If the simulated motion is non-pulse-like, the parameters ($\alpha_{NP1}, \beta_{NP1}, c_{NP1}, t_{max,q,NP1}, f_{mid,NP1}, f'_{NP1}, \zeta_{f,NP1}$) and ($\alpha_{NP2}, \beta_{NP2}, c_{NP2}, t_{max,q,NP2}, f_{mid,NP2}, f'_{NP2}, \zeta_{f,NP2}$) of the major and intermediate ground motion components are used to generate the horizontal components of a non-pulse-like near-fault ground motion in the major and intermediate “principal” directions α_{NP1} and $\alpha_{NP2} = \alpha_{NP1} + 90^\circ$, respectively.

For a given earthquake scenario ($F, M_w, Z_{TOR}, R_{RUP}, V_{s30}, s_{or}d, \theta_{or}\phi$), the procedure described in Steps 1 to 3 can be repeated to generate as many synthetic near-fault ground motions as necessary. The simulated components can be rotated into any desired direction, eg, to match the orientation of the axes of a structure of interest. The type (pulse-like or non-pulse-like), the model parameters, and the underlying white-noise processes of the MFW model vary from simulation to simulation. As a result, the simulated motions are variable and should be viewed as resulting from different earthquakes that have common source and site characteristics. These simulated motions have the same natural variability that is present in the database of recorded near-fault ground motions that was used to fit the model parameters.

10 | POSTPROCESSING OF SIMULATED ACCELERATION TIME SERIES

Each synthetic acceleration time series generated from the MFW process described in Section 3.2 is low-cut filtered using a fourth-order acausal Butterworth filter applied in the frequency domain. The filter has a magnitude dependent cutoff frequency f_c , in Hz,

$$\log_{10} f_c = 1.41 - 0.345 M_w. \quad (15)$$

This postprocessing is necessary to ensure that the corresponding velocity and displacement time series return to zero at the end of the shaking, and to control the low-frequency content of the synthetics in a manner consistent with the physics of real earthquake events. This postprocessing is different from the one applied to synthetic far-field ground motions in Rezaeian and Der Kiureghian.^{43,44} For more details, see Dabaghi and Der Kiureghian.^{4,37}

11 | VALIDATION OF SIMULATED MOTIONS

11.1 | Comparison with recorded motions

To validate the simulation procedure for specified earthquake source and site characteristics, we compare synthetic motions to recorded motions in terms of their time series and elastic response spectra. We simulate 5 pairs of horizontal components of pulse-like motions for the earthquake scenario ($F = 0, M_w = 6.53, Z_{TOR} = 0 \text{ km}, R_{RUP} = 0.1 \text{ km}, V_{s30} = 265 \text{ m/s}, s_{or}d = 19.5 \text{ km}, \theta_{or}\phi = 5.4^\circ$), which is similar to the scenario for the pulse-like record NGA#171 (1979

Imperial Valley-06 earthquake–El Centro-Meloland Geotechnical Array station) in the NGA-West2 database. For this scenario, the predicted probability of observing a pulse in any direction is calculated in (13) to be 0.63; non-pulse-like ground motions may also occur but are not considered in this example. A discretization step $\Delta t = 0.005$ second and a low-cut filter cutoff frequency $f_c = 0.144$ Hz calculated from (15) are used.

Figure 3 shows the acceleration, velocity, and displacement time series of the recorded (black) and simulated (gray) motions in the direction of the largest pulse and in the orthogonal horizontal direction. Model parameters values fitted to record NGA#171 and those randomly generated for the 5 synthetic motions are listed in the figure. The predicted median values directly obtained from the mean predictive relations are also listed. Figure 3 (bottom left) shows the elastic pseudoacceleration response spectra at 5% damping of the recorded (black) and simulated (gray) ground motions. For each case, a peak is observed in the response spectrum of the largest pulse component at periods longer than 1 second. These peaks generally occur at or slightly below the period of the corresponding mMP velocity pulse.

For the same earthquake scenario, the simulated model parameter values, pulse-like ground motion time series, and spectral shapes show significant variability in the intensity, duration, and frequency content characteristics. The spectra of the recorded motion fall within the range of variability of the spectra of the simulated motions. However, the recorded motion has much smaller spectral amplitudes than most of the 5 simulated motions. This is because the recorded components have Arias intensities that are much smaller than expected, on the average, from a pulse-like near-fault ground motion of the given earthquake source and site characteristics. The recorded and simulated motions should be viewed as possible realizations of pulse-like ground motions resulting from different earthquakes that have common source and site characteristics; the variability observed reflects the randomness that is inherent in the ground motion parameters for the given set of earthquake source and site characteristics.

Furthermore, Figure 3 (bottom right) shows elastic pseudoacceleration response spectra at 5% damping for 100 other simulated ground motion components (gray lines), their median (dashed lines), and their median plus and minus one standard deviation levels (dotted lines). Note that the spectra of the recorded components fall within the ranges spanned by the spectra of the simulated components at all periods, and mostly within one standard deviation range.

11.2 | Comparison with NGA-West2 GMPEs

Another validation exercise is to compare the statistics of the elastic response spectra of synthetic ground motions with those of recorded ground motions, as described by the NGA-West2 GMPEs, keeping in mind the limitations of these GMPEs in the near-fault region. In fact, the earthquake scenarios used in the NGA-West2 GMPEs do not include the directivity parameters $s_{or}d$ and $\theta_{or}\phi$ nor do they differentiate between FD and BD sites. Moreover, these GMPEs were calibrated to records from ranges of magnitude and distance that are much larger than those of the dataset used in this study, and they make no distinction between pulse-like and non-pulse-like motions. Thus, their regression models may be driven by the large amount of mostly non-pulse-like ground motions recorded at larger distances. As a result, these GMPEs may be less well calibrated to ground motions from larger magnitude earthquakes (5.5–8.0) and at shorter distances (0–31 km), to which our model is limited.

We use a weighted average of the 5 NGA-West2 models³⁵ developed by (1) Abrahamson, Silva, and Kamai (ASK14)⁵⁹; (2) Boore, Stewart, Seyhan, and Atkinson (BSSA14)⁶⁰; (3) Campbell and Bozorgnia (CB14)³⁶; (4) Chiou and Youngs (CY14)⁶¹; and (5) Idriss (I14).⁶² Following the recommendation in Rezaeian et al,⁶³ all models are assigned a weight of 2/9 except I14, which is assigned a weight of 1/9. These GMPEs were developed for the orientation-independent RotD50 spectrum.⁶⁴ At each period, the RotD50 spectrum gives the median spectral acceleration over all horizontal orientations; it may arise from different orientations at different periods. Hereafter, the weighted average of the 5 NGA-West2 GMPEs is denoted the NGA-West2 model.

Synthetic motions are compared with GMPEs for 3 hypothetical earthquakes that occur on vertical strike-slip faults ($F = 0$) with $Z_{TOR} = 0$ and have magnitudes $M_w = 6.5, 7,$ and 7.5 . Two sites are considered, having $V_{s30} = 760$ m/s and $V_{s30} = 525$ m/s, both located at $R_{RUP} = 10$ km from the fault rupture. The 6 ($F, M_w, Z_{TOR}, R_{RUP}, V_{s30}$) earthquake scenarios are summarized in Table 10. For the input parameters that remain unspecified in the various GMPEs, default values are assigned.

To generate synthetic motions for each ($F, M_w, Z_{TOR}, R_{RUP}, V_{s30}$) scenario, 15 hypocenter locations and 40 sites having the same V_{s30} and all located at the same distance R_{RUP} from the fault rupture are considered. The 15 hypocenter locations are assumed to have a uniform distribution along the strike of the fault, except for buffer zones of length 0.1 times

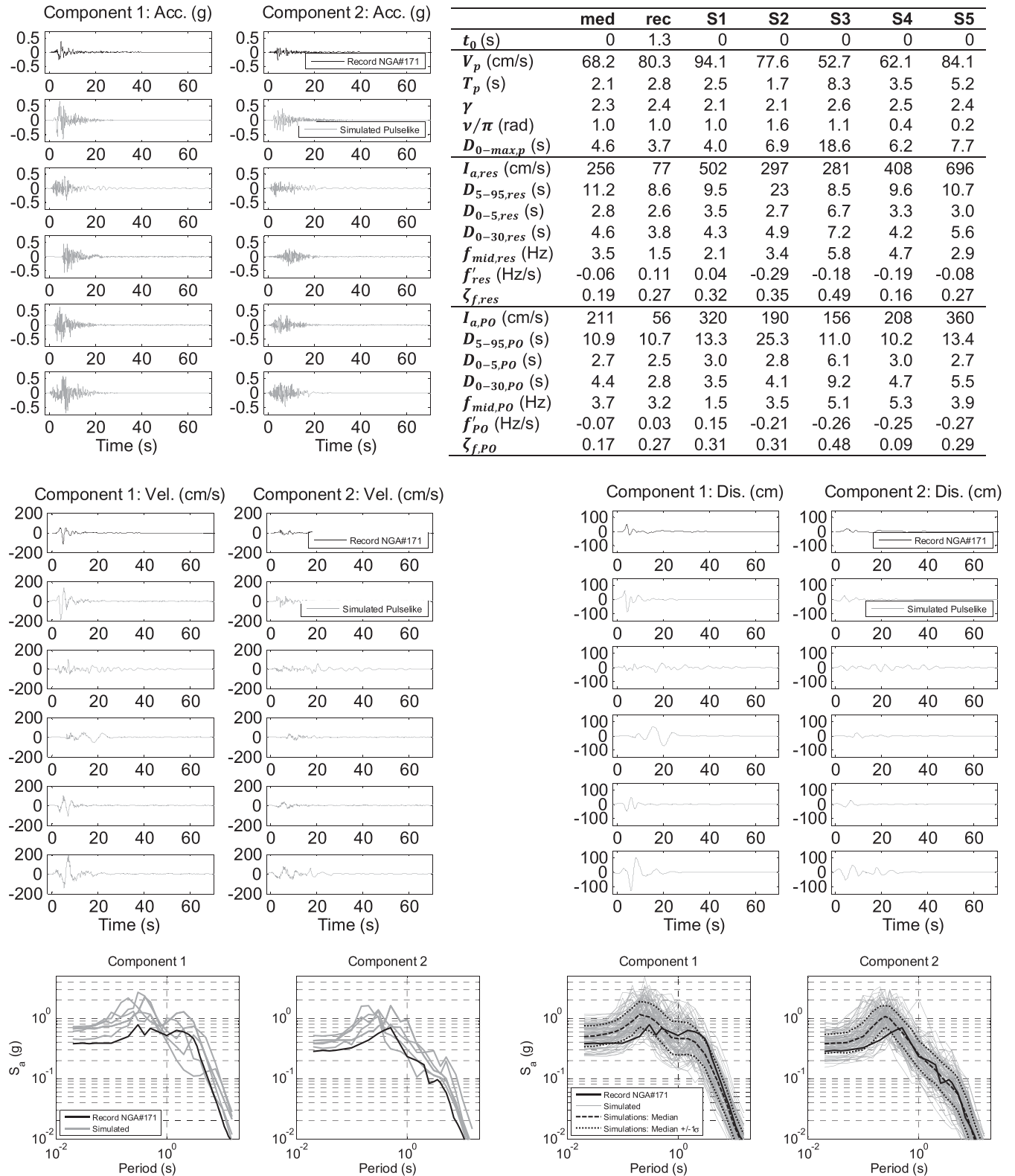


FIGURE 3 Recorded (black) and simulated (gray) horizontal pulse-like near-fault ground motion components in the direction of the largest pulse (component 1) and the corresponding orthogonal direction (component 2) for the prescribed earthquake source and site characteristics of record NGA#171 (1979 Imperial Valley-06 earthquake–El Centro-Meloland Geotechnical Array station): acceleration, velocity, and displacement time series; model parameters; and 5% damped pseudoacceleration response spectra with 5 (left) and 100 (right) simulated motions are shown

TABLE 10 Description of earthquake scenarios used for comparison of our stochastic model with NGA-West2 GMPEs

F	M_w	Z_{TOR} , km	R_{RUP} , km	V_{s30} , m/s	Directivity	s or d , km	θ or ϕ , °	Pr(pulse-like), %	
1	0	6.5	0	10	760	RD	0–26	0–90	21.3
						FD	26	0	38.4
						BD	0	90	5.3
2	0	7.0	0	10	760	RD	0–53	0–90	28.4
						FD	53	0	51.5
						BD	0	90	5.3
3	0	7.5	0	10	760	RD	0–108	0–90	39.2
						FD	108	0	69.4
						BD	0	90	5.3
4	0	6.5	0	10	525	RD	0–26	0–90	21.3
						FD	26	0	38.4
						BD	0	90	5.3
5	0	7.0	0	10	525	RD	0–53	0–90	28.4
						FD	53	0	51.5
						BD	0	90	5.3
6	0	7.5	0	10	525	RD	0–108	0–90	39.2
						FD	108	0	69.4
						BD	0	90	5.3

the rupture length at both ends of the fault, where the rupture length is predicted as a function of magnitude using the mean relation developed by Wells and Coppersmith.⁶⁵ The 40 sites are uniformly distributed at R_{RUP} from the fault rupture. The resulting 600 hypocenter-site combinations constitute a representative range of the possible rupture directivity conditions ($s_{or}d$, $\theta_{or}\phi$) with appropriate likelihoods for the given earthquake scenario; the ranges are listed in Table 10. For each ($s_{or}d$, $\theta_{or}\phi$) scenario, one synthetic ground motion is generated using the procedure of Section 9. The 600 synthetic motions obtained represent the random directivity (RD) condition for the corresponding (F , M_w , Z_{TOR} , R_{RUP} , V_{s30}) scenario. The average probability of observing a pulse in the ground motion considering all possible directivity conditions is calculated from (13) and listed in Table 10. Note that this probability does not depend on V_{s30} .

For each of the 6 (F , M_w , Z_{TOR} , R_{RUP} , V_{s30}) earthquake scenarios, Figure 4 compares the statistics of the 5% damped pseudoacceleration response spectra of the corresponding 600 synthetic RD motions with those described by the NGA-West2 model. The statistics compared are the median and median plus and minus one logarithmic standard deviation levels for the RotD50 horizontal component. The median spectra predicted by each of the 5 NGA-West2 GMPEs are also shown to illustrate the variability between models. Although GMPEs predict spectral values only up to 10 seconds, the spectra of simulated motions are plotted up to a period of 20 seconds to illustrate the effect of the directivity pulses in simulated pulse-like motions, since a few of these pulses have periods longer than 10 seconds.

In general, Figure 4 shows good agreement between the synthetics and the GMPEs. At most periods for each scenario, the median spectrum of the RD simulated motions falls within or near the boundary of the range spanned by the median spectra of the 5 GMPEs. Moreover, the median level from the simulated motions falls within the median plus and minus one standard deviation levels predicted by the NGA-West2 model. And despite the tendency of our simulations to predict larger spectral ordinates at periods greater than 1 or 2 seconds, especially for scenarios 1 and 3, the difference is not major. This difference at the longer periods may indicate that our model over predicts longer periods, and/or that the NGA-West2 GMPEs do not adequately represent the near-fault rupture directivity effect.

An important feature of the proposed simulation procedure is its ability to account for the source-to-site geometry and to differentiate between FD and BD sites. To illustrate this feature, for each earthquake scenario, 2 distinct cases of ($s_{or}d$, $\theta_{or}\phi$) among the directivity scenarios considered are examined in more detail, representing the 2 extremes of rupture directivity, namely, maximum FD and BD. The corresponding values of ($s_{or}d$, $\theta_{or}\phi$) and of the probability of observing a pulse are listed in Table 10. For each FD or BD scenario, 300 synthetic motions are generated; this number is found to provide a relatively stable estimate of the statistics of the response spectra for a given (F , M_w , Z_{TOR} , R_{RUP} , V_{s30} , $s_{or}d$, $\theta_{or}\phi$) scenario.

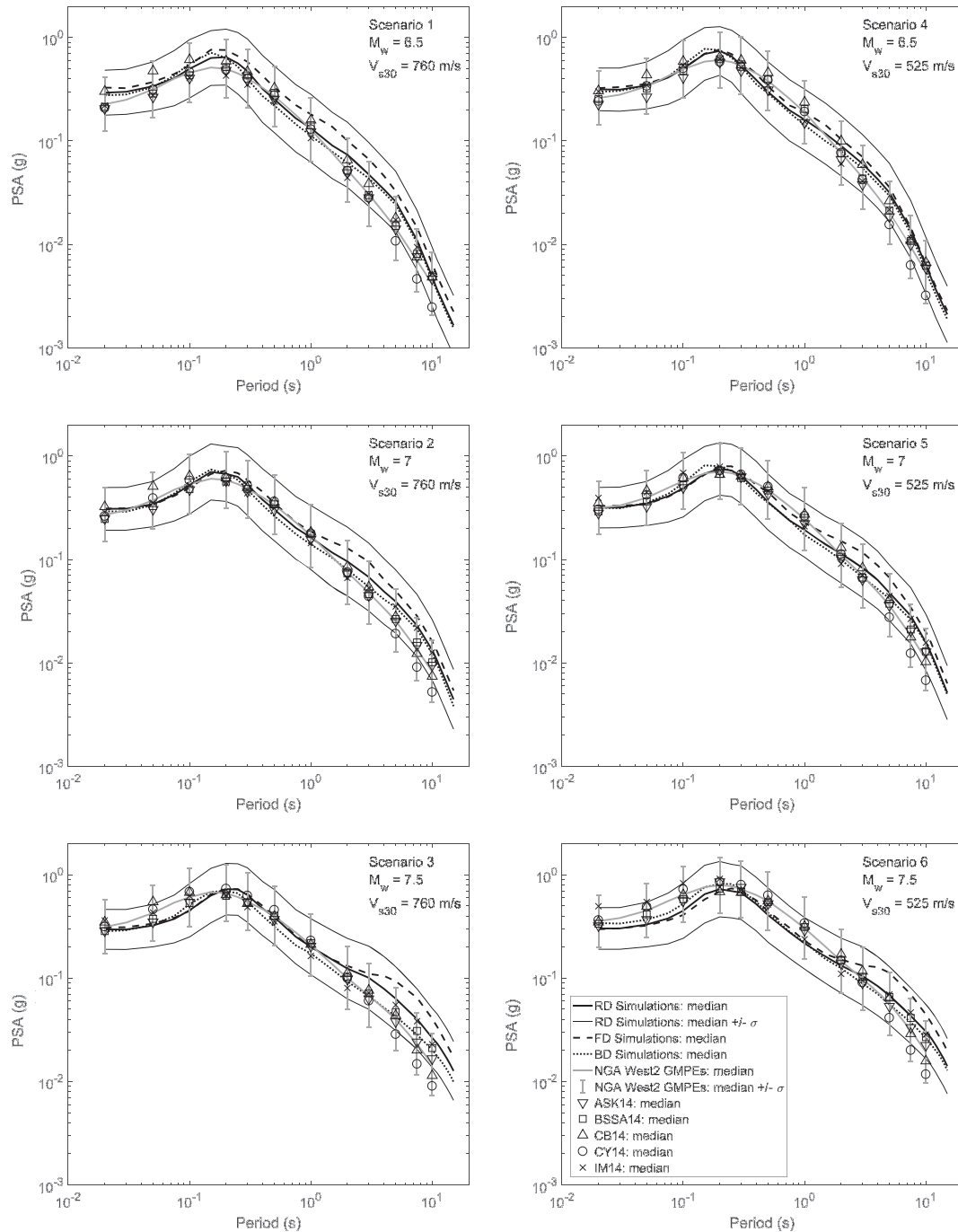


FIGURE 4 Median and median plus and minus one logarithmic standard deviation of 5% damped pseudoacceleration response spectra of RotD50 component for 600 random directivity (RD) synthetic motions, median spectra for 300 forward directivity (FD) and 300 backward directivity (BD) synthetic motions, median and median plus and minus one logarithmic standard deviation spectra predicted by a combination of the 5 NGA-West2 GMPEs, and median spectra predicted by each of the 5 NGA-West2 GMPEs for different earthquake scenarios: $M_w = 6.5$ (top), $M_w = 7.0$ (middle), and $M_w = 7.5$ (bottom); $V_{s30} = 760$ m/s (left) and $V_{s30} = 525$ m/s (right). All scenarios have $F = 0$, $Z_{TOR} = 0$ km, $R_{RUP} = 10$ km

For each $(F, M_w, Z_{TOR}, R_{RUP}, V_{s30})$ scenario, Figure 4 also compares the median of the 5% damped pseudoacceleration response spectra of synthetic ground motions for FD and BD conditions with those obtained from RD conditions. It can be seen that the median spectral values at longer periods are largest for the FD scenarios and lowest for the BD scenarios, with the RD median spectral values lying in between. These differences occur because pulse-like motions are most frequent and have longer periods at FD sites. Except for scenario 3, the BD spectrum lies close to (mostly slightly below) the

RD spectrum. The differences between the RD, FD, and BD spectra are largest for the $M_w = 7.5$ scenarios because of the large differences in their corresponding pulse probabilities (see Table 10). Note that the median of the BD simulations, only 5% of which are pulse-like, also exceeds the NGA-West2 model at the longer periods, especially for scenario 1. However, it lies within the range of the individual GMPEs. Again, this indicates that our model may over predict longer periods, and/or that the NGA-West2 GMPEs may be biased at shorter distances.

Finally, a comparison of the logarithmic standard deviations of the RotD50 spectra from the simulated RD motions and from the GMPEs finds them to be generally comparable between periods of 0.1 and 10 seconds. This demonstrates that the proposed simulation procedure maintains the natural variability of ground motions for a given set of earthquake source and site characteristics. At periods below 0.1 second, the variability of the simulated motions is smaller than that predicted by GMPEs and this difference is also observed in Figure 4. However, these short periods do not influence the response of typical structural systems of interest.

In summary, the results indicate that the proposed simulation procedure produces near-fault ground motion time series that are realistic and more or less consistent with existing GMPEs for different earthquake scenarios. The differences, which are smaller than the variability in the GMPEs themselves, may indicate that our model over predicts longer periods, and/or that the NGA-West2 GMPEs do not adequately represent the near-fault rupture directivity effect. An important feature of our simulation procedure is its ability to include directivity effects and to differentiate between different source-to-site geometries. Nonetheless, the discrepancies between the simulations and the NGA West2 model at the longer periods require further investigation.

12 | CONCLUSION

A novel procedure to simulate suites of synthetic near-fault ground motions for specified earthquake source and site characteristics is proposed. The procedure requires inputting values of earthquake source and site parameters that are readily available to design engineers and generates 2 horizontal orthogonal components of both pulse-like and non-pulse-like near-fault ground motions.

The proposed procedure uses previously developed stochastic models of pulse-like and non-pulse-like near-fault ground motion.^{4,37} These models are fitted to recorded ground motions in 2 databases, one for pulse-like and another for non-pulse-like motions, taken from PEER's NGA-West2 database. Using the "observed" data of identified model parameters, regression and correlation analyses are performed to develop predictive models of the parameters of the stochastic models in terms of a small number of earthquake source and site parameters, namely, $(F, M_w, Z_{TOR}, R_{RUP}, V_{S30}, s_{or}d, \theta_{or}\phi)$. A random-effect model is used to account for the correlation arising from multiple records from some earthquakes. The uncertainty in the model parameters and the statistical correlations between them are taken into account to capture the natural variability of real ground motions. To the extent possible, the functional forms of the predictive equations are selected to be consistent with seismological theory and with similar relations used for GMPEs by other researchers. One important advantage of the proposed relations is that they make the crucial distinction between pulse-like and non-pulse-like ground motions.

The proposed simulation procedure can be used to generate synthetic near-fault ground motions from shallow crustal earthquakes in active tectonic regions for any prescribed earthquake scenario specified by the set of parameters $(F, M_w, Z_{TOR}, R_{RUP}, V_{S30}, s_{or}d, \theta_{or}\phi)$ within the boundaries of the databases used, preferably for $6 \leq M_w \leq 7.5$, $5 < R_{RUP} \leq 25$ km, and $400 < V_{S30} < 1000$ m/s. The probability of occurrence of a directivity pulse is first computed using the pulse probability model in Shahi and Baker.³⁴ Pulse-like and non-pulse-like bidirectional horizontal ground motions are simulated according to the predicted proportions. For each type of motion, the predictive equations are used to simulate realizations of the respective model parameters. These are then used to generate a corresponding synthetic near-fault ground motion. The orientation of the simulated ground motion components is predicted using empirical pulse-like and non-pulse-like directionality models also developed herein.

To provide validation of the proposed models and simulation procedure, examples of synthetic ground motions are compared with recorded motions in terms of their acceleration, velocity, and displacement time series and elastic response spectra. The comparison shows that the synthetic motions possess realistic characteristics and preserve the natural variability of real ground motions. Moreover, suites of synthetic ground motions generated for given earthquake source and site characteristics are compared with the NGA-West2 GMPEs in terms of median elastic response spectra and associated variability. In contrast with the NGA-West2 GMPEs, which do not include a directivity model, the proposed simulation procedure accounts for both pulse-like and non-pulse-like ground motions and allows distinction

between FD and BD scenarios through directivity parameters $s_{or}d$ and $\theta_{or}\phi$. As a result, the simulations are able to represent the differences at longer periods between the response spectra at FD and BD sites. Median spectra of synthetic ground motions at BD sites are overall in good agreement with the corresponding median spectra predicted by the NGA-West2 GMPEs. For FD sites, median spectra show higher amplitudes in the long-period range than the GMPE spectra. For average or RD conditions, good agreement is observed in general between the simulations and the GMPEs. However at the longer periods, the median levels from the simulations generally lie above the median yet below the median plus one standard deviation levels from the GMPEs. This difference at the longer periods may indicate that our model over predicts longer periods, and/or that the NGA-West2 GMPEs do not adequately represent the near-fault rupture directivity effect and do not properly account for the contribution of pulse-like motions. Importantly, the simulations exhibit variability in elastic response spectral amplitudes that is consistent at most periods of interest with that predicted by the NGA-West2 GMPEs.

The present study can easily be extended to also simulate the vertical component of ground motion. Moreover, a model of the fling step can easily be incorporated into the proposed model formulation and simulation procedure for sites located adjacent to the fault rupture that undergo permanent static ground displacement; see Dabaghi and Der Kiureghian³⁷ for examples.

ACKNOWLEDGEMENTS

This study was sponsored by the Pacific Earthquake Engineering Research Center (PEER) and funded by the California Department of Transportation (Caltrans) under Contract No. 59A0582, by the Pacific Gas & Electric Company, and through Funds 96829 and 18081 of the PEER Transportation Systems Research Program. Any opinions, findings, and conclusions or recommendations expressed in this writing are those of the authors and do not necessarily reflect those of the sponsoring agencies. Additional support was provided by the Taisei Chair in Civil Engineering at the University of California, Berkeley. We thank Yousef Bozorgnia, Tom Shantz, Sanaz Rezaeian, and Nico Luco for their helpful feedback and suggestions during the course of this study. Special thanks also go to Tadahiro Kishida for valuable data and processing results and to Jack Baker and Shrey Shahi for their pulse-extraction codes and results, as well as for their consultation during the course of this study. Finally, we thank 2 anonymous reviewers for their feedback and comments, which have improved the paper.

ORCID

Mayssa Dabaghi  <http://orcid.org/0000-0003-2017-3462>

REFERENCES

1. Archuleta RJ, Hartzell SH. Effects of fault finiteness on near-source ground motion. *Bull Seismol Soc Am*. 1981;71(4):939-957.
2. Somerville PG, Smith NF, Graves RW, Abrahamson NA. Modification of empirical strong ground motion attenuation relations to include the amplitude and duration effects of rupture directivity. *Seismol Res Lett*. 1997;68(1):199-222. <https://doi.org/10.1785/gssrl.68.1.199>
3. Mavroeidis G, Papageorgiou A. Near-source strong ground motion: characteristics and design issues, *Proceedings, Proc. of the Seventh US National Conf. on Earthquake Engineering (7NCEE), Boston, Massachusetts, 2002*.
4. Dabaghi M, Der Kiureghian A. Stochastic model for simulation of near-fault ground motions. *Earthq Eng Struct Dyn*. 2017;46(6):963-984. <https://doi.org/10.1002/eqe.2839>
5. Bertero VV, Mahin SA, Herrera RA. Aseismic design implications of near-fault San Fernando earthquake records. *Earthq Eng Struct Dyn*. 1978;6(1):31-42. <https://doi.org/10.1002/eqe.4290060105>
6. Champion C, Liel A. The effect of near-fault directivity on building seismic collapse risk. *Earthq Eng Struct Dyn*. 2012;41(10):1391-1409. <https://doi.org/10.1002/eqe.1188>
7. Sehhati R, Rodriguez-Marek A, Elgawady M, Cofer WF. Effects of near-fault ground motions and equivalent pulses on multi-story structures. *Eng Struct*. 2011;33(3):767-779. <https://doi.org/10.1016/j.engstruct.2010.11.032>
8. Kalkan E, Kunnath SK. Effects of fling step and forward directivity on seismic response of buildings. *Earthq Spectra*. 2006;22(2):367-390. <https://doi.org/10.1193/1.2192560>
9. Chopra AK, Chintanapakdee C. Comparing response of SDF systems to near-fault and far-fault earthquake motions in the context of spectral regions. *Earthq Eng Struct Dyn*. 2001;30(12):1769-1789.

10. Mavroeidis GP, Dong G, Papageorgiou AS. Near-fault ground motions, and the response of elastic and inelastic single-degree-of-freedom (SDOF) systems. *Earthq Eng Struct Dyn*. 2004;33(9):1023-1049. <https://doi.org/10.1002/eqe.391>
11. Graves R, Jordan TH, Callaghan S, et al. CyberShake: a physics-based seismic hazard model for southern California. *Pure Appl Geophys*. 2011;168(3-4):367-381.
12. Luco N, Mai P, Cornell C, Beroza G. Probabilistic seismic demand analysis at a near-fault site using ground motion simulations based on a stochastic-kinematic earthquake source model, *Proceedings, 7th U.S. National Conference on Earthquake Engineering*, Boston, MA, 2002.
13. Bazzurro P, Cornell C. Vector-valued probabilistic seismic hazard analysis (VPSHA). *Proceedings of the 7th US national conference on earthquake Engineering 2002*; 21-25.
14. Beck J, Papadimitriou C. Moving resonance in nonlinear response to fully nonstationary stochastic ground motion. *Probabilist Eng Mech*. 1993;8(3-4):157-167.
15. Bray JD, Rodriguez-Marek A. Characterization of forward-directivity ground motions in the near-fault region. *Soil Dyn Earthq Eng*. 2004;24(11):815-828. <https://doi.org/10.1016/j.soildyn.2004.05.001>
16. Shahi SK, Baker JW. An empirically calibrated framework for including the effects of near-fault directivity in probabilistic seismic hazard analysis. *Bull Seismol Soc Am*. 2011;101(2):742-755. <https://doi.org/10.1785/0120100090>
17. Dreger D, Hurtado G, Chopra A, Larsen S. Near-field across-fault seismic ground motions. *Bull Seismol Soc Am*. 2011;101(1):202-221. <https://doi.org/10.1785/0120090271>
18. Liu T, Luan Y, Zhong W. A numerical approach for modeling near-fault ground motion and its application in the 1994 Northridge earthquake. *Soil Dyn Earthq Eng*. 2012;34(1):52-61. <https://doi.org/10.1016/j.soildyn.2011.11.001>
19. Mavroeidis GP, Papageorgiou AS. A mathematical representation of near-fault ground motions. *Bull Seismol Soc Am*. 2003;93(3):1099-1131.
20. Halldórsson B, Mavroeidis GP, Papageorgiou AS. Near-fault and far-field strong ground-motion simulation for earthquake engineering applications using the specific barrier model. *J Struct Eng*. 2011;137(3):433-444. [https://doi.org/10.1061/\(ASCE\)ST.1943-541X.0000097](https://doi.org/10.1061/(ASCE)ST.1943-541X.0000097)
21. Motazedian D, Atkinson GM. Stochastic finite-fault modeling based on a dynamic corner frequency. *Bull Seismol Soc Am*. 2005;95(3):995-1010. <https://doi.org/10.1785/0120030207>
22. Fu Q, Menun C. Seismic-environment-based simulation of near-fault ground motions, *Proceedings, 13th World Conference on Earthquake Engineering*, 2004.
23. Yang D, Zhou J. A stochastic model and synthesis for near-fault impulsive ground motions. *Earthq Eng Struct Dyn*. 2014;44(2):243-264. <https://doi.org/10.1002/eqe.2468>
24. Lungu A, Giaralis A. A non-separable stochastic model for pulse-like ground motions, *Proceedings, 11th International Conference on Structural Safety and Reliability, ICOSSAR 2013*, Columbia University New York, NY, 2013.
25. Broccardo M, Der Kiureghian A. Simulation of near-fault ground motions using frequency-domain discretization, *Proceedings, 10th National Conference on Earthquake Engineering*, Anchorage, AK, 2014.
26. Pitarka A, Somerville P, Fukushima Y, Uetake T, Irikura K. Simulation of near-fault strong-ground motion using hybrid Green's functions. *Bull Seismol Soc Am*. 2000;90(3):566-586. <https://doi.org/10.1785/0119990108>
27. Papageorgiou AS, Aki K. A specific barrier model for the quantitative description of inhomogeneous faulting and the prediction of strong ground motion. I. Description of the model. *Bull Seismol Soc Am*. 1983;73(3):693-722.
28. Krawinkler H, Alavi B. Development of improved design procedures for near-fault ground motions, *Proceedings, SMIP98, seminar on utilization of strong motion data*, Oakland, CA, 1998.
29. Mukhopadhyay S, Gupta VK. Directivity pulses in near-fault ground motions—I: identification, extraction and modeling. *Soil Dyn Earthq Eng*. 2013;50:1-15. <https://doi.org/10.1016/j.soildyn.2013.02.017>
30. He W-L, Agrawal AK. Analytical model of ground motion pulses for the design and assessment of seismic protective systems. *J Struct Eng*. 2008;134(7):1177-1188.
31. Somerville P. Development of an improved representation of near fault ground motions, *Proceedings, SMIP98 Seminar on Utilization of Strong-Motion Data*, 1998.
32. Mukhopadhyay S, Gupta VK. Directivity pulses in near-fault ground motions—II: Estimation of pulse parameters. *Soil Dyn Earthq Eng*. 2013;50(Complete):38-52. <https://doi.org/10.1016/j.soildyn.2013.02.019>
33. Cork TG, Kim JH, Mavroeidis GP, Kim JK, Halldórsson B, Papageorgiou AS. Effects of tectonic regime and soil conditions on the pulse period of near-fault ground motions. *Soil Dyn Earthq Eng*. 2016;80:102-118.
34. Shahi SK, Baker JW. An efficient algorithm to identify strong-velocity pulses in multicomponent ground motions. *Bull Seismol Soc Am*. 2014;104(5):2456-2466.
35. Bozorgnia Y, Abrahamson NA, Atik LA, et al. NGA-West2 research project. *Earthq Spectra*. 2014;30(3):973-987. <https://doi.org/10.1193/072113EQS209M>

36. Campbell KW, Bozorgnia Y. NGA-West2 ground motion model for the average horizontal components of PGA, PGV, and 5% damped linear acceleration response spectra. *Earthq Spectra*. 2014;30(3):1087-1115.
37. Dabaghi M, Der Kiureghian A. Stochastic modeling and simulation of near-fault ground motions for performance-based earthquake engineering, *PEER Report No. 2014/20*, Pacific Earthquake Engineering Research Center, University of California, Berkeley, CA, 2014.
38. Somerville P, Graves R. Conditions that give rise to unusually large long period ground motions. *Struct Des Tall Build*. 1993;2(3):211-232. <https://doi.org/10.1002/tal.4320020304>
39. Somerville PG. Characterizing near fault ground motion for the design and evaluation of bridges, *Proceedings, Third National Conference and Workshop on Bridges and Highways*, Portland, Oregon, 2002.
40. Somerville P. Seismic hazard evaluation, *Proceedings, 12th World Conference on Earthquake Engineering*, Auckland, New Zealand, 2000.
41. Baker JW. Quantitative classification of near-fault ground motions using wavelet analysis. *Bull Seismol Soc Am*. 2007;97(5):1486-1501. <https://doi.org/10.1785/0120060255>
42. Dabaghi M, Rezaeian S, Der Kiureghian A. Stochastic simulation of near-fault ground motions for specified earthquake and site characteristics, *Proceedings, 11th International Conference on Applications of Statistics and Probability in Civil Engineering*, Zurich, Switzerland, 2011.
43. Rezaeian S, Der Kiureghian A. A stochastic ground motion model with separable temporal and spectral nonstationarities. *Earthq Eng Struct Dyn*. 2008;37(13):1565-1584.
44. Rezaeian S, Der Kiureghian A. Simulation of synthetic ground motions for specified earthquake and site characteristics. *Earthq Eng Struct Dyn*. 2010;39(10):1155-1180. <https://doi.org/10.1002/eqe.997>
45. Spudich P, Rowshandel B, Shahi SK, Baker JW, Chiou BSJ. Comparison of NGA-West2 directivity models. *Earthq Spectra*. 2014;30(3):1199-1221. <https://doi.org/10.1193/080313EQS222M>
46. Iervolino I, Cornell CA. Probability of occurrence of velocity pulses in near-source ground motions. *Bull Seismol Soc Am*. 2008;98(5):2262-2277.
47. Boore DM, Goulet CA. The effect of sampling rate and anti-aliasing filters on high-frequency response spectra. *Bull Earthq Eng*. 2014;12(1):203-216.
48. Shahi SK. A probabilistic framework to include the effects of near-fault directivity in seismic hazard assessment. *PhD Thesis, Dept. of Civil and Environmental Engineering*, Stanford University, Stanford, CA, 2013.
49. Abrahamson NA. Statistical properties of peak ground accelerations recorded by the SMART 1 array. *Bull Seismol Soc Am*. 1988;78(1):26-41.
50. Jayaram N, Baker JW. Statistical tests of the joint distribution of spectral acceleration values. *Bull Seismol Soc Am*. 2008;98(5):2231-2243.
51. Rathje EM, Faraj F, Russell S, Bray JD. Empirical relationships for frequency content parameters of earthquake ground motions. *Earthq Spectra*. 2004;20(1):119-144. <https://doi.org/10.1193/1.1643356>
52. Kempton JJ, Stewart JP. Prediction equations for significant duration of earthquake ground motions considering site and near-source effects. *Earthq Spectra*. 2006;22(4):985-1013.
53. Bommer JJ, Stafford PJ, Alarcón JE. Empirical equations for the prediction of the significant, bracketed, and uniform duration of earthquake ground motion. *Bull Seismol Soc Am*. 2009;99(6):3217-3233.
54. Rezaeian S, Der Kiureghian A. Stochastic modeling and simulation of ground motions for performance-based earthquake engineering, *PEER Report No. 2010/02*, Pacific Earthquake Engineering Research Center, University of California, Berkeley, CA, 2010.
55. Brillinger DR, Preisler HK. Further analysis of the Joyner-Boore attenuation data. *Bull Seismol Soc Am*. 1985;75(2):611-614.
56. Abrahamson N, Youngs R. A stable algorithm for regression analyses using the random effects model. *Bull Seismol Soc Am*. 1992;82(1):505-510.
57. Campbell KW, Bozorgnia Y. NGA ground motion model for the geometric mean horizontal component of PGA, PGV, PGD and 5% damped linear elastic response spectra for periods ranging from 0.01 to 10 s. *Earthq Spectra*. 2008;24(1):139-171.
58. Campbell KW, Bozorgnia Y. A ground motion prediction equation for the horizontal component of cumulative absolute velocity (CAV) based on the PEER-NGA strong motion database. *Earthq Spectra*. 2010;26(3):635-650.
59. Abrahamson NA, Silva WJ, Kamai R. Summary of the ASK14 ground motion relation for active crustal regions. *Earthq Spectra*. 2014;30(3):1025-1055.
60. Boore D, Stewart J, Seyhan E, Atkinson G. Summary of the BSSA14 GMPE. *Earthq Spectra*. 2014;30:
61. Chiou BS-J, Youngs RR. Update of the Chiou and Youngs NGA model for the average horizontal component of peak ground motion and response spectra. *Earthq Spectra*. 2014;30(3):1117-1153.
62. Idriss I. An NGA-West2 empirical model for estimating the horizontal spectral values generated by shallow crustal earthquakes. *Earthq Spectra*. 2014;30(3):1155-1177.

63. Rezaeian S, Petersen MD, Moschetti MP, Powers P, Harmsen SC, Frankel AD. Implementation of NGA-West2 ground motion models in the 2014 US National Seismic Hazard Maps. *Earthq Spectra*. 2014;30(3):1319-1333.
64. Boore DM. Orientation-independent, nongeometric-mean measures of seismic intensity from two horizontal components of motion. *Bull Seismol Soc Am*. 2010;100(4):1830-1835. <https://doi.org/10.1785/0120090400>
65. Wells DL, Coppersmith KJ. New empirical relationships among magnitude, rupture length, rupture width, rupture area, and surface displacement. *Bull Seismol Soc Am*. 1994;84(4):974-1002.

How to cite this article: Dabaghi M, Der Kiureghian A. Simulation of orthogonal horizontal components of near-fault ground motion for specified earthquake source and site characteristics. *Earthquake Engng Struct Dyn*. 2018;47:1369–1393. <https://doi.org/10.1002/eqe.3021>